Professor Dawson's pioneering work in computer simulations of space and astrophysical plasmas

Bertrand Lembège, J.N. Leboeuf, P. Liewer, M. Ashour-Abdalla

CENTRE NATIONAL D'ETUDES DES TELECOMMUNICATIONS

CENTRE NATIONAL DE LA RECHERCHE SCIENTIFIQUE

CENTRE DE RECHERCHES EN PHYSIQUE DE L'ENVIRONNEMENT TERRESTRE ET PLANETAIRE

CRPE

NOTE TECHNIQUE
CRPE/191

PROFESSOR DAWSON's PIONEERING WORK IN COMPUTER SIMULATIONS OF SPACE AND ASTROPHYSICAL PLASMAS

Par

B. LEMBEGE *RPE/OPN 38/40, rue du Général Leclerc, 92131 Issy-les-Moulineaux*

J.N. LEBOEUF *Oak Ridge National Laboratory, Oak Ridge (USA)*

P. LIEWER *JPL, Pasadena (USA)*

M. ASHOUR-ABDALLA *UCLA, IGPP, Los Angeles (USA)*

RPE/OPN
38-40, rue du Général Leclerc
92131 ISSY-LES-MOULINEAUX, FRANCE

CENTRE NATIONAL D'ETUDES
DES TELECOMMUNICATIONS
Centre Paris B

CENTRE NATIONAL DE LA
RECHERCHE SCIENTIFIQUE
Département TOAE

**CENTRE DE RECHERCHES EN PHYSIQUE DE
L'ENVIRONNEMENT TERRESTRE ET PLANETAIRE**

NOTE TECHNIQUE CRPE/191

PROFESSOR DAWSON's PIONEERING WORK IN COMPUTER SIMULATIONS OF SPACE AND ASTROPHYSICAL PLASMAS

par

B. LEMBEGE
RPE/OPN
38-40 rue du Général Leclerc, 92131 Issy-les-Moulineaux
J.N. LEBOEUF
Oak Ridge National Laboratory, Oak Ridge (USA)
P. LIEWER
JPL, Pasadena (USA)
ASHOUR-ABDALLA
UCLA, IGPP, Los Angeles (USA)

Le Directeur

G. SOMMERIA

Le Directeur Adjoint

J.J. BERTHELIER

Mars 1991

LISTE DE DIFFUSION SYSTEMATIQUE

CNET

MM.	FENEYROL	Directeur du CNET
	THABARD	Directeur Adjoint du CNET
	COLONNA	Adjoint Militaire au Directeur du CNET
	MEREUR	Directeur des Programmes
	BLOCH	DICET
	THUE	DICET
MME	HENAFF	DICET
MM.	PIGNAL	PAB
	RAMAT	PAB
	ZYLBERSZTEJN	PAB-BAG
	ABOUDARHAM	PAB-SHM
	HOCQUET	PAB-STC
	THEBAULT	PAB-STS
MME	PARIS	PAB-RPE
MM.	BAUDIN	PAB-RPE
	BERTHELIER	PAB-RPE
	BIC	PAB-RPE
	CERISIER	PAB-RPE
	GENDRIN	PAB-RPE
	LAVERGNAT	PAB-RPE
	ROBERT	PAB-RPE
	ROUX	PAB-RPE
	SOMMERIA	PAB-RPE
	TESTUD	PAB-RPE
	VIDAL-MADJAR	PAB-RPE

CNRS

MM.	BERROIR	TOAE
	CHARPENTIER	SPI
MME	SAHAL	TOAE
MM.	COUTURIER	INSU
	CADET	INSU

CNES

MMES	AMMAR
	DEBOUZY
MM.	BAUDOIN
	FELLOUS
	HERNANDEZ (Toulouse)

EERM

. ANDRE

MEN/DRED

M. MEGIE

Bibliothèques

CNET-SDI (3)
CNET-EDB
CNET-RPE (Issy) (5)
CNET-RPE (St Maur) (2)
Observatoire de Meudon
CNRS-SA
CNRS-INIST
CNRS-LPCE

LISTE COMPLEMENTAIRE

CCETT	DOCUMENTATION
LAA/SLC/BSA	HERVE
LAB/IFE/COD	LE MOIGNE 2 EX
LAB/SHR/TCM	LE CORRE
PAA/LEA/AGH	SEBASTIEN
PAB/RPE/OPN	CANU
PAB/RPE/TID	LEBLANC

EXTERIEUR

ENST BR	DOCUMENTATION

PROFESSOR DAWSON's PIONEERING WORK IN COMPUTER SIMULATIONS OF SPACE AND ASTROPHYSICAL PLASMAS

by

B. Lembège[1], J.N. Leboeuf[2], P. Liewer[3]

and M. Ashour-Abdalla[4]

(1) CRPE/CNET, 92131 Issy-les-Moulineaux Cedex (France)
(2) Oak Ridge National Laboratory, Oak Ridge (USA)
(3) JPL, Pasadena (USA)
(4) UCLA, IGPP, Los Angeles (USA)

ABSTRACT

This paper is a non-exhaustive review of John Dawson's research work in the domain of space plasma simulation. Its includes some of his most significant contributions brought on physics of auroral phenomena, on magnetospheric physics as well as solar physics and astrophysics. In many opportunities, Professor Dawson has developped a pioneering work in terms of development of new global MHD and particle codes, with innovative applications to the physics of space plasma phenomena. Finally, the interest of Professor Dawson in the new architectures of highly parallel super-computers will be presented and illustrated by simulation results obtained recently.

AVANT - PROPOS

Cet article de revue a été rédigé dans le cadre du Symposium "John DAWSON" qui s'est déroulé dans les Catalina Islands (24-25 Septembre 1990, USA) en l'honneur des 60 ans du Professeur J.M. DAWSON, responsable du groupe de simulation numérique au Département de Physique de l'Université de Californie de Los Angeles (UCLA). Ce document paraîtra dans le livre "From Fusion to Light Surfing: Lectures on Plasma Physics honoring John M. DAWSON", Ed. T. KATSOULEAS, Addison-Wesley Publi. Company, USA, (parution prévue : Mai 1991).

This review has been written for the "John DAWSON Symposium" held in Catalina Islands (September 24-25, 1990), for honoring the 60th birthday of Professor DAWSON, head of the numerical simulation group at the Physics Department of UCLA (Los Angeles, USA). This report will be published with others in the dedicated book "From Fusion to Ligth Surfing: Lectures on Plasma Physics honoring John DAWSON", Ed. T. KATSOULEAS Addison-Wesley Publi. Company, USA, (expected issue : May 1991).

I - INTRODUCTION

This paper presents a review of some illustrative simulation results that Professor Dawson brought in space plasma physics. Participating in honoring John Dawson is a significant honor in itself but, such a review is not an easy task, because of the abundant and continuous flow of innovative ideas that Professor Dawson has provided and of studies achieved through many years in various domains of space plasma simulations. Then, this review looks much like a typical "*coktail*" offered for Professor Dawson's birthday than like a systematic review of all his work developped in this domain. We hope that the reader will forgive us for such choice and the "*non-exhaustive*" aspect of this review. We have chosen to concentrate only on a few important results that Professor Dawson has obtained and/or which he has largely contributed to, in order to emphasize his pioneering work in simulations of space plasma ; moreover, several of these works illustrate quite well his continuous effort spent for establishing a link between fusion and space communities.

The content of this review has been structured as follows :

1) Global simulations of the time-dependent magnetosphere

2) Particle simulations of kinetic instabilities in space plasmas

3) "Forays" in particle simulations of astrophysical plasmas

4) Particle simulations of nonlinear magnetosonic waves and magnetosonic shocks in space plasmas.

5) Simulations of relativistic particles in a strongly magnetized plasma

6) Particle simulations on new architectures of highly parallel supercomputers : an application to magnetospheric shocks

and conclusions, illustrating the particular importance of numerical simulation in the domain of space plasma physics, will close this review.

II - GLOBAL SIMULATIONS OF THE TIME-DEPENDENT MAGNETOSPHERE

As far as the earth's magnetosphere is concerned, the lack of global information characteristic of laboratory experiments stems from the experimental inability to "photograph" the magnetosphere and the theoretical inability to solve the nonlinear time dependent three-dimensional (3D) magnetohydrodynamic (MHD) and plasma equations describing the magnetosphere. Laboratory, and more appropriately here, numerical simulations can potentially bridge this gap and allow theorists to go beyond what was once referred to, by Roald Sagdeev, as the "Cartoon Approximation" in constructing global models of the earth's interaction with the solar wind.

In point of fact, circa 1977, Prof. Charles Kennel came back to UCLA from the USSR where he had occasion to discuss results from laboratory experiments, performed by Prof. Podgorny's group and which attempted to reproduce the interaction of the solar wind with the earth (e. g. Podgorny, Dubinin, Izraelevich, Potanin, 1977) . Unexpectedly, these laboratory experiments were showing a different magnetospheric topology depending on the solar wind Alfven Mach number M_A. For $M_A < 2.5$, the classic Dungey (1961) picture of the magnetosphere could be reproduced, but for $M_A \geq 10$ the dayside reconnection region was moving to the polar cusps. Prof. Kennel then asked the seminal question: *why not carry out similar experiments on the computer?.*

It so happened that we had developed a one-of-a-kind particle magneto-hydrodynamic simulation code (Leboeuf, Tajima, Dawson, 1979) which we thought could be readily modified to handle such situations. The first model was two-and-one-half dimensional (2-1/2D or two space and three velocities dimensions) with the solar wind modeled as a plasma stream in the x-y plane, carrying its own northward or southward magnetic field if desired.The earth was modeled by a dipole magnetic field produced by a pair of oppositely flowing currents out of the plane in the z-direction, which were kept constant throughout the time-dependent simulations. In the particle MHD model, elements of the fluids are treated as finite size particles. The particle quantities such as position, mass and momentum are advanced in a Lagrangian way while the magnetic fields are calculated in an Eulerian manner. The position of each j particle making up the fluid is calculated by :

$$d\vec{r}_j/dt = \vec{v}_j \qquad (1)$$

$$d\vec{v}_j/dt = -1/\rho[\vec{\nabla}P + 1/8\pi\vec{\nabla}B^2 - 1/4\pi\vec{\nabla}.\vec{B}\vec{B}] \qquad (2)$$

The plasma is modeled as an ideal two-dimensional (2-D) MHD fluid with an adiabatic equation of state so that

$$T/n^{\gamma-1} = \text{constant} \tag{3}$$

The density is in turn expressed as

$$n(r_g) = \sum_j f(r-r_j) \tag{4}$$

where $f(r-r_j)$ is the form factor of the particle, typically a gaussian one.

The magnetic fields are updated at the mesh points as follows

$$\partial\vec{B}/\partial t = \vec{\nabla} \times (\vec{v}_g \times \vec{B}) + \eta_{num} \nabla^2 \vec{B} \tag{5}$$

where the fluid velocity $\vec{v}_g$ is defined as

$$\vec{v}_g(r) = \sum_j \vec{v}_j(r)\, f(r-r_j) / \sum_j f(r-r_j) \tag{6}$$

The resistive term η_{num} in the magnetic field equation (Eq. 5) is of numerical origin and is due to the fact that we use the diffusive Lax scheme to integrate the magnetic field in time. It gives rise to an effective Lundquist number of 10-20 for the magnetospheric simulations discussed here. This numerical resistivity was all but eliminated in subsequent improvements to the particle MHD model (Brunel, Leboeuf, Tajima, Dawson, Makino, Kamimura, 1981). It turns out to be a blessing here because it allows for easy reconnection of magnetic field lines.

Deceptively simple and highly resistive as it was, the computer model yielded a wealth of , at that time unexpected, physics results (Leboeuf, Tajima, Kennel, Dawson, 1978 and 1979). In the absence of solar wind magnetic field, an essentially closed "teardrop" magnetosphere is produced. Appearance of the density compression associated with the bow shock, of the density maximum in the magnetosheath over the polar caps, the formation of a low density cavity in the downstream region and the inhomogeneous high density region near and within the magnetopause are all within theoretical expectations and in agreement with in-situ observations. More importantly, the simulations reveal that the shock front, magnetosheath, and magnetopause were fluttering with a time period and scalelength that could be explained by a Kelvin-Helmholtz instability generated at the shock, the magnetopause or both. This prediction is now generally accepted as an experimental fact.

With a steady southward solar wind magnetic field, the first question the computer model answered by letting the time-dependent simulations evolve to a quasi-steady state was that the classical Dungey picture of the reconnected, open magnetosphere with neutral

lines in the nose and tail persisted for $M_A \geq 10$, contrary to the laboratory experiments. With a steady-state northward solar wind magnetic field, a teardrop like magnetospheric configuration was produced with neutral lines over the polar cusps.

Since the topology of the magnetosphere depended on the solar wind field orientation, we postulated that a "substorm" was the time dependent adjustment of magnetosperic topology resulting from the sudden rotation of the upstream solar wind magnetic field. A "substorm" would correspond to a southward rotation. We then proceeded to exploit fully the time-dependent nature of the simulations and modelled a substorm as the passage of a rotational continuity over the magnetosphere which switches the solar wind field from east-west to southward. Results from such a simulation are shown in Figure 1, where magnetic field lines are plotted in the x-y plane of the calculations. The initial solar wind magnetic field is everywhere uniform and parallel to the geomagnetic equatorial plane. At time t=0, the solar wind field suddenly rotates southward at x=0. The rotational discontinuity thereafter propagates inward along x at the speed of the fluid, which has a fast Mach number M_F=2.5. In the top frame of Figure 1, the discontinuity has approached the nose of the magnetosphere and apparently initiated reconnection there. In the middle frame of Figure 1, the discontinuity is passing over the polar caps. Note that tail reconnection has been initiated and that a bubble of closed flux has formed downstream. In the bottom frame of Figure 1, the discontinuity has passed beyond the far edge of the diagram, and the magnetosphere has arrived at a Dungey configuration.

The most interesting features of our time-dependent simulations were the prediction of the formation of a bubble of closed flux which would propagate downstream during a magnetospheric substorm. This prediction was dramatically confirmed in 1984 by observations with the ISEE 3 spacecraft in the magnetotail 220 RE from earth, of plasmoids, bodies of plasma and closed magnetic loops, passing that location in clear delayed response to substorms (Hones, Baker, Bame, Feldman, Gosling, Mc Comas, Zwickl, Slavin, Smith, Tsurutani, 1984).

Our ability to model the time dependent magnetosphere in three dimensions was severely limited by the available computational ressources. Our necessarily low resolution, first attempt (Leboeuf, Tajima, Kennel, Dawson, 1981) using a three-dimensional extension of our particle MHD model did however demonstrate the feasibility of such calculations. It was successful in reproducing the steady-state Dungey topology in three dimensions. It revealed some interesting features which were absent in our 2D simulations. In particular, it showed the formation of a compression zone downstream of the tail neutral line, probably bounded by wake shocks, whose cross-section was also changing with distance downstream.

These first global simulations of the magnetosphere have been followed by many others at UCLA and elsewhere. The activity has in fact grown into a field of research in its own right, supplementing today's more sophisticated means of experimental observations and more elaborate nonlinear theoretical methodology.

III - PARTICLE SIMULATIONS OF KINETIC INSTABILITIES IN SPACE PLASMAS

One of the inherent difficulties of interpreting spacecraft observations related to waves and particle distribution functions in space plasmas is that the time resolution is too coarse to resolve the much shorter time scales over which kinetic instabilities might occur in the particular region of space under scrutiny. The ingenuity of the theorist is put to the test since one has to be able to infer from postulated initial conditions what the nonlinear saturated states of the plasma might be, given that the spacecrafts probe the plasma in its steady state. These problems can however readily be attacked by means of particle simulations.

3.1. Heating of cold electrons by odd half-harmonic cyclotron waves

Such a challenge was presented to us by what have come to be known as "odd half-harmonic" electron cyclotron emissions since their frequency $\omega \approx (n+1/2)\ \omega_{ce}$. Satellite observations of electric field fluctuations in the magnetosphere were showing intense oscillations at these frequencies during the diffuse aurorae (Gurnett, Scarf, Fredricks, Smith, 1978).

Linear theory had shown that a combination of a weak loss cone distribution for hot electrons (of plasma sheet origin) and a Maxwellian distribution for the less dense, cold electron population (of ionospheric origin) was unstable to the growth of electrostatic electron cyclotron waves at frequencies $\omega \approx (n+1/2\ )\omega_{ce}$.

Two saturation scenarios had also been advanced. The first was relying on resonance broadening to neutralize the effect of the hot electron free energy source. The second was advocating that the cold electrons would be heated nonlinearly, would change the nature of the instability from non-convective to convective and the waves would saturate by propagating out of the unstable region.

Our particle simulation study of these cyclotron harmonic waves was undertaken with two objectives in mind; first to determine the saturation mechanism and second, to see if the cold electrons could be heated and if so, by what mechanism (Ashour-Abdalla, Leboeuf, Dawson, Kennel, 1980).

A standard 2-1/2D electrostatic finite size particle simulation code was used, with the electrons described by particles moving in the x-y plane under the action of the Lorentz

force and the ions constituting a neutralizing background of charges. The particle equations of motion for the electrons are :

$dx/dt=v_x$

$dy/dt=v_y$

$d\vec{v}/dt = -|e|/m(\vec{E}+\vec{v}/c \times \vec{B}_0)$

with $\vec{v} = (v_x, v_y, v_z)$

were supplemented by a solution of Poisson's equation on a grid in (x,y) space

$\vec{\nabla} . \vec{E} = -4\pi |e| (n_e - n_0)$

with the electronic number density accumulated in the same way as in Eq. 4 for the particle MHD code described earlier .

The simulation was started with a distribution known to be unstable to the growth of electron cyclotron harmonic waves. The hot electrons free energy source was taken to be a hot ring distribution in velocity space perpendicular to the magnetic field with ring velocity $v_b=5v_{te}$, i.e five times the thermal velocity of the hot electrons (with Maxwellian distribution parallel to the magnetic field). The cold electrons component was chosen to have a density 25% that of the hot electrons and a Maxwellian velocity distribution function in all three velocity dimensions with temperature 100 times colder than for the hot electrons. The magnetic field strength was chosen such that the ratio of electron cyclotron frequency to electron plasma frequency was $\omega_{ce}/\omega_{pe}=0.3$.

The many results from these simulations are perhaps best illustrated by Figure 2, where the location of hot and cold particles are plotted in the velocity space v_z-v_y perpendicular to the magnetic field in the x-direction. In the top frame of Figure 2, the dense ring of hot electrons, shown in red, and the dilute cold electrons (meant to be blue but appropriately showing up as white) are clearly visible at the initial time. Between the top and middle frame of Figure 2, the wave energy increases linearly. Time series analysis shows that two waves are growing with frequencies $\omega_0 \approx 3/2\ \omega_{ce}$. Heating of the cold electrons, giving rise to the expanding blue cloud, is apparent in the middle frame of Figure 2. It is difficult to detect any change at that point in the hot electrons population. The waves saturate at that time and thereafter decay slighlty. The bottom frame of Figure 2 shows the distribution of magnetospheric electrons in the nonlinear saturated state, with the hot electrons having lost some of their free energy and the cold electrons having been heated further. There is still enough of a positive slope left in the hot electron distribution

function for it to be unstable according to linear theory, indicating that growth is being balanced by some nonlinear damping mechanism

The identification of the heating mechanism for the cold electrons and of the wave saturation mechanism led to some interesting detective work. Heating of the particles can only take place if the particles resonate with the waves. Initially, the cold electrons have a thermal velocity $v_{Tc} \approx 0.1\ v_{Te}$, and the smallest resonant velocity with the waves (the cyclotron one) is $v_{/\!/} = (\omega_0 - \omega_{ce})/\ k_{/\!/} = 1.5\ v_{Te}$, with $k_{/\!/}$ the component of the wavevector parallel to the magnetic field, so that the cold particles do not immediately resonate with the waves. The following scenario does however emerge. Initially the cold electrons are set into oscillations (no temperature increase) in both the perpendicular and parallel directions by the electric field of the growing wave. When $v_{/\!/}$ reaches a value such that cyclotron resonance can occur ($v_{/\!/} = 1.5\ v_{Te}$), then the cold temperature should increase in the direction perpendicular to the magnetic field. The hot electrons do not participate in this interaction since the effect of the waves is averaged out over their larger Larmor radius. Careful temperature and particle orbit diagnostics actually confirmed this picture and the calculated wave amplitude needed to bring the cold electrons into resonance did indeed match the measured value of the electric field in the simulation. We therefore concluded that the nonlinear onset of cyclotron resonance was the cause of saturation of the unstable electron cyclotron harmonic waves and the cause of the heating of the cold particles.

3.2. Velocity Space Shell Instabilities

We applied essentially the same techniques to a study of electrostatic velocity space shell instabilities in magnetized plasmas (Sentman, Leboeuf, Katsouleas, Huff, Dawson, 1986). This work was motivated by satellite observations which showed that dayside magnetospheric electron distributions detected at low latitudes simultaneously with the occurence of intense upper hybrid (UHR) noise could take the form of hot shells in velocity space (Kurth, Frank, Ashour-Abdalla, Gurnett, Burek, 1980). While these are more stable than ring distributions, addition of a colder background can render otherwise stable shell distributions unstable to cyclotron waves.

Our particle simulation model was identical to the one used for studying ring distributions with a colder background, same for the hot electron distribution which was modeled as a shell in velocity space. We found that both resonant and nonresonant (i.e. for which $k_{/\!/} = 0$) instabilities could occur. Saturation of the resonant instabilities was caused by nonlinear cyclotron resonance with the colder background (as for the ring distributions

simulated previously). We ultimately found that the non-resonant instabilities were saturating due to nonstochastic cyclotron harmonic damping by the cold background.

While these simulations have intrinsic scientific merit, the reason they are mentionned here is somewhat different. It is mainly because in the search and in the identification of the saturation mechanism for the nonresonant shell instabilities, we litterally stumbled across the $\vec{v} \times \vec{B}$ detrapping mechanism (Dawson, Decyk, Huff, Jechart, Katsouleas, Leboeuf, Lembege, Martinez, Ohsawa, Ratliff, 1983) which has had enormous impact on other works at UCLA. Even though $\vec{v} \times \vec{B}$ detrapping turned out to be irrelevant in the end for the shell instabilities we were studying, a detailed investigation of the mechanism in its relativistic rendition sparked the invention of the Surfatron concept of laser plasma acceleration by Katsouleas and Dawson (1983). Identification of the $\vec{v}\times\vec{B}$ detrapping mechanism as the dominant limiting factor in wave amplitude (Lembège, Ratliff, Dawson, Ohsawa, 1983) has also lead to significant advances in the understanding of magnetosonic shocks in space and astrophysical plasmas as detailed in Secs. V and VI.

Application of particle simulation techniques to space plasmas has been pursued vigorously ever since at UCLA. The work is having an ongoing impact in the interpretation of spacecraft observations and in predicting the outcome of particular events or perturbative spacecraft experiments.

IV - "FORAYS" IN PARTICLE SIMULATIONS OF ASTROPHYSICAL PLASMAS

There is probably no other medium in plasma physics where experimental verification of theoretical ideas is more difficult, if feasible at all, than in astrophysical plasmas. It is also a medium where theoretical inventiveness can be exerted freely and where one's intuition could be best guided or confirmed by numerical experiments.

One area of interest in the early 1980's concerned ultrarelativistic waves. They are ultrarelativistic in the sense that the quiver velocity, imparted by their electromagnetic field E oscillating at frequency $\omega \approx kc$ to a particle of rest mass m_j , $eE/m_j\omega$ far exceeds the speed of light c. These waves are thought to occur in the outer magnetosphere of pulsars and it has also been argued that their magnetospheres may be largely positronic plasmas. The plasma can in any case be treated as an electron-positron one since, for ultrarelativistic waves, the ion quiver momentum is large and the difference between electron and ion rest masses becomes insignificant.

For reasons of analytical tractability, theoretical work had been limited to using nonlinear fluid equations which only have a closed form when the plasma is assumed cold (zero temperature) in the presence of relativistic waves (Kennel, Fujimura, Pellat, 1979). It is however unrealistic to assume this, since such strong waves are expected to cause highly nonlinear wave-particle interactions. It thus appeared to us that computer simulations using particles would provide a powerful tool to investigate such problems, particularly since no time-dependent kinetic analysis of nonlinear relativistic waves had yet been carried out.

Our fully self-consistent electromagnetic particle codes with relativistic dynamics were readily put to the task. These types of particle simulation models consist of the following particle equations :

$$d\vec{p}_j/dt = q_j[\vec{E} + \vec{v}_j/c \times \vec{B}] \tag{7}$$

with the momentum for each j particle related to the velocity by

$$\vec{p}_j = \gamma_j m_j \vec{v}_j \tag{8}$$

$$\gamma_j = (1 + p_j^2/m_j^2c^2)^{1/2} \tag{9}$$

$$d\vec{r}_j/dt = \vec{v}_j \tag{10}$$

and field equations

$$\vec{\nabla} \times \vec{E} = -1/c \; \partial \vec{B} / \partial t \tag{11}$$

$$\vec{\nabla} \times \vec{B} = 1/c \; \partial \vec{E} / \partial t + 4\pi/c \, \vec{J} \tag{12}$$

$$\vec{\nabla} \cdot \vec{E} = 4\pi\rho \tag{13}$$

$$\vec{\nabla} \cdot \vec{B} = 0 \tag{14}$$

To be truly relativistic, the finite size particles should undergo Lorentz contraction. This would make the form factor $f(r-r_j)$, as used in Eq. 4 for example, a function of velocity. This complicates the calculations but can be done if the particles are not strongly relativistic. If they are strongly relativistic, the Lorentz contraction can become so large that the particle size in the direction of motion becomes much smaller than the grid spacing. However, the interpolation scheme of the particles to the grid, on which the field evaluations are carried out, automatically expands the particle to a grid size, so true contraction beyond this is possible. To our knowledge, such corrections have not yet been included in any calculations; however, for strongly relativistic situations, the codes appear to give reasonably accurate results agreeing with theory where checks can be made.

Our first particle simulation work on ultrarelativistic waves in electron-positron plasmas was stimulated by concurrent research in the beat wave laser plasma accelerator concept. In this acceleration scheme, an intense, spatially localized pulse of laser light impinging on the plasma leaves behind a wake of plasma waves which in turn accelerate particles to energies estimated to be in the GeV range (Tajima and Dawson, 1979). In an electron-positron plasma, the absence of charge separation precludes the existence of the wake of plasma waves and the acceleration mechanism, if present, would have to be different. Our simulations of the propagation of a linearly polarized ultrarelativistic pulse in positronic plasmas (Ashour-Abdalla, Leboeuf, Tajima, Dawson, Kennel, 1980) were performed in one space dimension but three velocities and electromagnetic field directions or 1-2/2 D. They show that particles can still be accelerated to very high energies. The acceleration stops when the bulk of the wave energy is converted to particle energy, with the maximum momenta achieved scaling as the square of the wave amplitude. The pulse leaves behind as a wake a vacuum region whose length scales as the amplitude of the wave. The results can be quantitatively explained by a simple snow plow or piston like action of the radiation on the plasma, therefore confirming the applicability of particle simulations to ultrarelativistic situations.

The second application concerned the existence of a nonlinear sawtooth wave solution, predicted by nonlinear fluid theory to be the likely outcome in steady-state of the interaction of ultrarelativistic waves with overdense electron-positron plasmas (Kennel,

Fujimura, Pellat, 1979). The following simple argument leads one to expect a sawtooth wave in steady state: for relativistic amplitudes, the current density is a square wave, which by integration of Ampere's law gives rise to a triangular or sawtooth-shaped magnetic field. The same code as was used for pulses can be applied to such initial, spatially extended waveforms. An electron-positron plasma with equal initial temperatures, cold or warm, is considered. The initial transverse electric and magnetic fields and particle momenta are chosen self-consistently. The input waveform is a sawtooth. The wave thereafter evolves self-consistently in space and time. The simulations show that the initial sawtooth, the nonlinear solution of the fluid equations, is destroyed in roughly one wave period and evolves into an unsteady wave modulated by spiky density and current perturbations. This is also true for a sinusoidal input waveform. Intense particle acceleration in the direction of propagation takes place, intense plasma heating is observed, and the system reaches a quasi-stationary state consisting of a heated forward propagating plasma containing a complex wave spectrum. A snapshot in this evolution is displayed in Figure 3 where the top frame clearly shows forward acceleration in the x component of the particle momenta. The initial sawtooth wave shape is barely recognizable in the y component of the momenta and in the z component of the transverse magnetic field.

As preliminary as they might have been, the ultrarelativistic pulse and sawtooth simulations showed that the original wave energy was rapidly converted to ultrarelativistic particles and waves. While pulses might be observable from the radiation of their accelerated particles in the pulsar environment or during star collapse to a neutral star or black hole, it seems likely that a single wave of immense amplitude will not exist long enough to be observable.

Application of particle simulation techniques to astrophysical situations clearly deserves to be pursued further. As limited as our attempts have been, the work is however proving useful in the interpretation of recent results showing acceleration of electrons and ions to relativistic energies by large amplitude, steepening magnetosonic waves (Sec. VI).

V - *PARTICLE SIMULATIONS OF NONLINEAR MAGNETOSONIC WAVES AND MAGNETOSONIC SHOCKS IN SPACE PLASMAS*

5.1. Particles acceleration and heating by low frequency waves ($\omega_{ci} < \omega < \omega_{lh}$).

One of the main applications of this study (initially developped for fusion purpose) to magnetospheric physics consists in establishing a possible correlation between the presence of ULF waves and of high energy ion distribution function simultaneoustly observed on board of GEOS satellite (Gendrin, 1985). Let us remind that GEOS has been the first spacecraft on which a sensitive three-component ULF antenna has been operating in a waveform mode in the whole frequency range from ~ 0.1 Hz to 10 Hz i.e. above and below the proton frequency f_{ci} ($f_{ci} \cong 1$ Hz at the geostationary orbit). In particular, two correlations have been found, as reported in Gendrin's review (1985) :

(a) during some magnetospheric wave events, the energetic proton distribution shows a structure in which there is a flux maximum both at a certain energy (of the order of 10 kev) and at 90° pitch angle (Perraut et al, 1982). Such a distribution can be roughly modeled by a ring of energetic protons to which an isotropic cold proton distribution is added. The frequency increase which occurs during the emission is probably due to the inward diffusion of the ring like distribution, the wave propagating outward to the spacecraft. This could be consistent with the fact the emission starts at the local proton gyrofrequency provided that it could be demonstrated that such waves can propagate only towards regions of lower gyrofrequencies,

(b) Korth et al. (1983, 1984) have also observed magnetosonic mawes (associated with wide band impulsive noise) in conjunction with displacements of energetic proton boundaries. The radial gradient in the energetic proton distribution is determined by the large East-West asymmetry observed during one spin period ; its characteristic length is of the order of a few gyradii ρ_i for ~ 20 keV protons.

In short, magnetosonic waves are often oberved in the equatorial magnetosphere, though their intensity is usually not large ($\leq$ 0.3 nT). Since they are generated near the proton gyrofrequency they could resonate with the thermal plasma provided they have a small but finite parallel wave number. Therefore, they could be at the origin of the heating of the thermal plasma of ionospheric origin to a few eV as is often observed (Décréau et al, 1982).

In order to establish the possible correlation between ion ring distribution and magnetospheric waves, a 1-2/2D fully electromagnetic, particle code (for both electrons and ions) has been used, where a magnetosonic wave is generated by applying an external

(non plasma) current $j_{oy} = j_o \sin(\omega t - kx)$ during the whole time length of the run and within the whole simulation box (Lembège et al, 1983 ; Lembège and Dawson, 1986).

The frequency ω and the wave-number k of the wave are chosen within the frequency range $\omega_{ci} < \omega < \omega_{lh}$, where ω_{lh} is the lower hybrid frequency. The nonlinear level of the pump wave is determined by the chosen value of the amplitude $|j_o|$. Two cases may be differenciated due to the quite different dynamics of ions and electrons, according to the propagation angle $\theta = (\vec{k}, \vec{B_o})$ between the wave vector and the magnetostatic field :

5.1.1. perpendicular propagation ($\theta = 90°$)

Numerical results have shown that a longitudinal electrostatic field $\tilde{E}_{lx}$ grows during the build up phase of the wave (due to the self-consistent space charge effects), and attains a nonlinear level which strongly distorts its shape so that many higher harmonics are produced. Ions are accelerated by this field and become trapped as soon as this acceleration is large enough so that the velocity of some accelerated ions reach the phase velocity $\tilde{v}_{\phi x}$ of the wave ($\tilde{v}_{xi} \equiv \tilde{v}_{\phi x}$), as evidenced in Figure 4 ; trapping loops clearly appear in Figure 4(i). This ion trapping has various consequences :

(i) it enhances the wave overtaking in both electrostatic and electromagnetic components (the wave crests overtaking the wave troughs),

(ii) it produces a large wave damping

(iii) while trapped, ions suffer an important $\vec{E} \times \vec{B}$ drift parallel to the wave front (y direction) which becomes large enough so that the detrapping force $q(\vec{v} \times \vec{B})$ balances the trapping force $q\vec{E}$; detrapped ions are ejected on a large Larmor orbit within the plane perpendicular to $\vec{B_o}$ and form a ring distribution,

(iv) this global 3-steps mechanism ,"acceleration - trapping - detrapping", is the source of an important ion heating perpendicular to $\vec{B_o}$; the energy transfer from the wave to the particles is well illustrated by the fact the ion heating becomes particularly large at the time the magnetosonic wave (both electrostatic and electromagnetic components respectively named $\tilde{E}_{lx}$ and $\tilde{E}_{ty}$, , $\tilde{B}_{tz}$) saturates because of the nonlinear damping (Figure 5). In contrast, electrons only suffer a poor heating by adiabatic compression as seen in Figure 4.

The formation of the ion ring is clearly evidenced in the 2D projection $(\tilde{p}_{xi}, \tilde{p}_{yi})$ of the 3-D plot of Figure 6 representing the ion phase space $(\tilde{p}_{xi}, \tilde{p}_{yi}, \tilde{x})$; the static field $\vec{B_o}$ is along z. The resulting ion heating is related to the well coherent motion of ions (non-stochastic heating) while they gyrate along the large Larmor orbit. Numerical results show

that this overall mechanism is still efficient for any wave frequency ω within the range $\omega_{ci} < \omega < \omega_{lh}$ (without any resonance constraint as $\omega = n\omega_{ci}$ or $\omega = \omega_{lh}$), provided a sufficient intensity of the wave is reached. Such results emphasize that ion ring can easily result from an interaction of magnetosonic wave with an ambiant plasma. However, experimental results obtained from GEOS have stressed that possible sources of magnetosonic waves could be the ion ring distribution itself (or steep radial gradients in the hot particle distribution) as noted by Gendrin (1985). Then, one can wonder if the resulting ion ring observed in the numerical simulations can lead to a "feed back" effect by relaxation and maintain a certain level of magnetosonic wave. This further point is still an open question since this mechanism could not be observed in the present results obtained with a 1-2/2 D code (i.e. 1D real space) ; further simulation using 2-1/2 D code (i.e. 2D real space) would be necessary to study the consequences of the ion ring relaxation and the new mechanisms of energy dissipation related to the additional dimension in the real space.

5.1.2. Oblique propagation ($90° > \theta > 45°$)

The next step was of course to determine the efficiency of the mechanism quoted above when θ departs from 90°. Similar plasma conditions have been used with the same simulation code (1-2/2 D) in order to study the interaction of a "pseudo-oblique" magnetosonic wave with the ambiant plasma (Lembège and Dawson, 1984a). The overall mechanisms may be summarized in terms of two new results :

(i) a strong ion heating and acceleration perpendicular to $\vec{B}_0$ still persist within an angular range $90° > \theta > \theta_{ti}$, where θ_{ti} is a critical angle below which the ion dynamics drops to very low level ; θ_{ti} was found to vary as $\pi/2 - \sqrt{m_e/m_i}$

(ii) an intense electron heating and acceleration take place for θ below a second critical angle θ_{te} (Figure 7). Such particles dynamics may be explained both by the dispersion properties and by geometrical effects. Indeed, both the phase velocity $v_{\phi x}$ and the group velocity defined for a given wave number increase when θ decreases ; this makes the ion trapping conditions ($v_{xi} \equiv v_{\phi x}$) more stringent than for $\theta = 90°$ and implies stronger ion heating if ions are trapped. For $\theta \leq \theta_{ti}$, ion trapping cannot take place any more and resulting ion heating drops to very low values. However, the situation largely differs for the electrons ; as θ decreases, the phase velocity parallel to $\vec{B}_0$, $v_{\phi//}$, (which is infinite for $\theta = 90°$) decreases while a small but finite component $E_{l//}$of the electrostatic field builds up. This results in appropriate conditions for electrons acceleration parallel to $\vec{B}_0$ and further trapping. For $\theta < \theta_{te}$, more and more electrons begin to be trapped, and some electron heating increases as θ decreases ($v_{\phi//}$ also decreases, which makes easier electron trapping), at the expense of the wave amplitude which suffers an important additional damping. Then, the electrons to a

large extent short out the E_{lx} field which, combined with the increasing $v_{\phi x}$ (more difficult ion trapping) and an increasing $E_{l//}$ (easier electron trapping) ,means that ion trapping is no longer possible below the critical angle θ_{ti} . As a consequence, three regimes may be defined according the angle θ (Figure 7) : the main part of the wave energy is transferred , (a) to ions for θ around 90°, (b) to both electrons and ions for $\theta_{te} > \theta > \theta_{ti}$ (with a particularly large energy transfer to electrons parallel to $\vec{B}_0$ since $\tilde{T}_{ze} >> \tilde{T}_{xe}$, $\tilde{T}_{ye}$) , and (c) only to electrons (isotropic heating since $\tilde{T}_{xe} \equiv \tilde{T}_{ye} \equiv \tilde{T}_{ze}$) for $\theta < \theta_{ti}$. In particular, an ion ring distribution persists as long as a certain number of accelerated ions succeed to be trapped and detrapped at later times within $90° > \theta > \theta_{ti}$.

It is of interest that the dissipation mechanisms discussed here apply to a broad range of frequencies when again no particular resonance is involved ($\omega_{ci} << \omega < \omega_\theta$, where $\omega_\theta = \omega_{lh}$ and ω_{ce} for the particular cases $\theta = 90°$ and $\theta = 0°$ respectively). These mechanisms can be involved to heat plasmas in many space phenomena (or in fusion systems) ; either ions or electrons or both can be heated.

5.2. *Magnetosonic shock*

A considerable amount of both experimental and numerical studies have been developped on magnetospheric shocks, in particular on the terrestrial bow shock located upstream of the magnetopause, as evidenced in previous reviews and monographs (Tidman and Krall, 1971 ; Biskamp, 1973 ; Sagdeev, 1979 ; Kennel et al., 1985 ; Goodrich, 1985 ; Quest, 1985 ; Papadopoulos, 1985 ; Burgess, 1987). This considerable effort has been largely motivated by the large amount of rich experimental data gathered on board of ISEE satellites. Since previous analysis have shown that shock behavior was mainly dominated by ion dynamics, a large part of the numerical effort has been based on the use of hybrid codes (electrons : massless fluid ; ions : particles) and has led to a net improvement in the understanding of the shock physics. Such codes are characterized by the fact that electron dynamics (i.e. the corresponding space and time scales) are neglected and the anomalous resistivity (generated by cross-field current instabilities) is included by a phenomenological adhoc parameter coupling the electron fluid equations and the ion particles pusher (Lorentz force). Such a procedure allows to follow the shock dynamics over long ion time scales and including large ion space scale, without following the electrons dynamics in details (Leroy and al, 1981, 1982 ; Winske and Leroy, 1984 ; Quest; 1986, 1989) ; this leads to an important saving of computational cost.

Professor Dawson was particularly interested in studying the shock dynamics but by using a fully particle code. In collaboration with Lembège, he started to study shocks in

conditions where the electrostatic field is mainly dictated by space charge effects (ω_{pe} / ω_{ce} $\leq$ 1) which is in contrast with the use of hybrid codes including the quasi-neutrality condition (approximation valid for ω_{pe} / ω_{ce} >>1). This point was of importance, since subcritical and supercritical shocks which are respectively defined by $M_A < M_A^*$ and $M_A > M_A^*$, (where M_A^* is the first critical Mach number) can be mainly characterized by important resistive and viscous dissipation respectively. How viscous dissipation varies from high to low M_A was not clarified until mid 80's ; in other words, since viscous dissipation is strongly associated with ion reflection, one can wonder how the amplitude of the electrostatic field at the shock front (which is responsible for this reflection) evolves for varying M_A. Such a question also leads to the necessity for comparing the shock features and the associated particle dynamics, in cases where the electrostatic field is strictly self consistent (particle code) or is imposed by $N_e = N_i$ condition (hybrid code). Another motivation was to determine carefully the characterictics of an oblique magnetosonic shock ($90° > \theta > 45°$) where the electrons dynamics (in particular parallel to $\vec{B}_0$), is expected to play an important role (Feldman, 1985).

Numerical studies of shocks based on the use of 1-2/2D fully particle, electromagnetic code have started at UCLA in 1984 (Lembège and Dawson , 1984b). As a first step, dynamics of magnetosonic shocks and of both associated particle species (electrons and ions) have been studied in details for a direction of propagation perpendicular to $\vec{B}_0$ (Lembège and Dawson, 1987a). Main numerical results obtained for various regimes of the shock may be summarized as follows :

(i) for a supercritical shock ($M_A > M_A^*$), an important number of uptream ions behave in a way similar to that quoted in Sec. V.1 and suffer a "3-steps mechanism" (acceleration-trapping-detrapping) at the shock front, which plays the role of an electrostatic as well as a magnetic barrier ; analogous ion dynamics is also observed at the overshoots of the downtream trailing wavetrain where the local electric field can be large enough to trigger some ion trapping. This interpretation of the ion dynamics through the shock front is not only a semantic difference with respect to the ion reflexion mechanism commonly referred in previous studies ; rather, it offers the possibility for determining carefully the resonant interaction range $\Delta\tilde{t} = \tilde{t}_{dt,i} - \tilde{t}_{tr}$ (between ion detrapping and trapping times), and then can be used as a support for determining the corresponding local wave damping and for a possible confrontation with analytical calculations.

Reflected ions describe very large Larmor orbits and form a ring distribution ; a large rapid non-stochastic ion heating results from this ion gyration. This heating is the main source of viscous dissipation and is responsible for large field damping. Reflected ions accumulate in front of the shock during their large gyration before

they get enough energy to be able to cross the shock front and propagate in the downstream region. This continuous accumulation leads to the formation of a foot which, in the present case, can largely grow in time and reach the level of the first magnetic overshoot ; then, it plays the role of a new front (Figure 8). While propagating, the shock front develops a self-reformation similar to that already observed by Biskamp and Welter (1972). This self-reformation mechanism not evidenced in the hybrid simulations is still a subject of controverse. In summary, three ion distributions can be distinguished (Figure 9) : a Maxwellian distribution of the uptream ions (peak P_1 of the unperturbed plasma), a drifted Maxwellian distribution of the directly transmitted ions (which succeed to pass freely through the shock and form the peak P_2), and a ring distribution of the reflected ions. At the end of a self-reformation cycle, a new ion ring starts building up as evidenced in Figure 9. In contrast, electrons poorly interact with the electrostatic field since $v_{thi} << v_{the} < v_\phi$ at time $\tilde{t} = 0$; they only suffer a weak adiabatic compression effect mainly at the locations where the ion density becomes large i.e. mainly at the foot (arrow f), at the shock ramp and at the overshoots of the downstream wavetrain (Figure 10) .

(ii) for a subcritical shock ($M_A < M_A^*$), the situation differs completely : the density of trapped-reflected ions drops to a low (but finite) value leading to a broad ion distribution function with a weak tail (instead of a ion ring). A weak adiabatic bulk ion heating results. The self-reformation of the shock does not take place clearly. Indeed, since the amplitude of the foot is much weaker (less reflected ions), its velocity is also weaker. Then, the foot cannot separate clearly in time from the front itself which overtakes it. In summary, the transition between high and low Mach regimes takes place through a certain range of M_A (instead of one critical value M_A^*), through which viscous dissipation (and associated perpendicular ion heating) drops from strong to weak values.

All the shocks characteristics quoted above have been obtained for strictly perpendicular propagation. An extensive study has been performed for oblique cases within the range ($90° > \theta > 45°$). In such cases, the electron dynamics may be important since the shock electric fields in the direction of propagation (along the normal $\vec{n}$ to the wave front) have a component along the magnetic field $E_{//} = E_n \cos\theta$, allowing the electrons as well as the ions to be accelerated by these large electric fields (Feldman, 1975 ; Lembège and Dawson, 1987b). As a consequence, a fluid treatment of electrons may be inadequate. Main simulation results including a kinetic treatment of electrons may be summarized as follows :

(a) critical angles θ_{ce} and θ_{ci} similar to those defined for the interaction of magnetosonic waves with an ambiant plasma (sect. V.1) have been recovered. Electron heating

and acceleration particularly large along $\vec{B}_o$ are observed for $\theta < \theta_{ce}$, while those for the ions are strong within the plane ($\perp_1$, $\perp_2$) perpendicular to $\vec{B}_o$. Perpendicular ion trapping, and consequent heating, dominates when θ is around 90° ($90° > \theta > \theta_{ll}$), and is mainly located at the shock front ; in contrast, electron trapping is dominant for smaller angles and takes place both at the shock front and in the downstream trailing wavetrain (Figure 11). Detrapping of ions reflected by the shock front limits their resonant interaction with the electrostatic field $\vec{E}_{lx}$ and restricts their acceleration along the direction parallel to the shock front during their trapping. In contrast, electrons primarily move parallel to $\vec{B}_o$ and do not suffer any detrapping ; they largely overshoot the parallel momentum of the shock. Then, an important electron current $\tilde{j}_{ez}$ results along the z direction and can be large enough to induce new electromagnetic component $\tilde{B}_{ty}$ and $\tilde{E}_{tz}$ (which are negligible for $\theta = 90°$) ; as a reference, $\vec{B}_o$ is along z direction when $\theta = 90°$ and $\vec{B}_o = (B_{ox} , O , B_{oz})$ for $\theta \neq 90°$.

(b) the electron acceleration along $\vec{B}_o$ (and the resulting plasma current) can be large enough to generate a whistler precursor which escape ahead of the shock front provided that θ deviates from 90° below a certain value : in other words, the shock front plays the role of an antenna and evacuates the forward propagating waves by radiation from the location where they are generated (Figure 12). The dispersion properties show that low and high wavenumbers defined for a given angle $\theta < \theta_{ce}$ correspond respectively to forward and backward propagating waves ; they are respectively at the origin of a precursor and a trailing wavetrain (Tidman and Krall, 1971).

(c) When $\theta < \theta_{ce}$, our numerical results have shown, for the first time to our knowledge, that a double layer pattern forms at the shock front and plays an important role in the shock dynamics (Lembège and Dawson , 1989a). Indeed, narrow trapping loops of energetic electrons take place parallel to $\vec{B}_o$. In contrast with ions, these energetic electrons are very sensitive to the field fluctuations due to their light mass. Hence, the narrow width $\Delta\tilde{x}_{le}$ of their trapping loops. Numerical results have indicated that $\Delta\tilde{x}_{le} << \Delta\tilde{x}_{li}$, which is the origin of a double layer parallel to $\vec{B}_o$, as seen in the profile of $\tilde{E}_{lx}$ (Figure 12) ; $\Delta\tilde{x}_{li}$ is the wide trapping loop of ions also accelerated parallel to $\vec{B}_o$. Moreover, electrons are strongly accelerated through this "self-maintained" double layer and are scattered off by ion and magnetic fluctuations behind the shock. The potential drop at the front is required to slow down the ions, and the electrons must also respond to this jump. In summary, for the ions the processes are more or less limited to the direction perpendicular to $\vec{B}_o$, while for electrons acceleration parallel to $\vec{B}_o$ and scattering perpendicular take place.

When detailed dynamics of both electrons and ions need to be included, long numerical runs covering a few ω_{ci}^{-1} can become very costly on "standard" supercomputers. Very early, Professor Dawson has pointed out this problem and has encouraged a few of us to engage some efforts in numerical applications on the new promising architectures of highly parallel supercomputers. Topic of oblique shocks represents a typical example for large computational needs and has been recently selected in this purpose, as described in Sect. VII.

VI - *SIMULATIONS OF RELATIVISTIC PARTICLES IN A STRONGLY MAGNETIZED PLASMA*

Acceleration of both electrons and ions to relativistic energy by large amplitude magnetosonic waves has been investigated in the case of a strongly magnetized plasma. Such a study may have various applications in the domain of solar physics as well as in astrophysics. Indeed, high amplitude electromagnetic waves may occur during solar flares events or in the outer magnetospheres of pulsars. In the case of solar physics, direct observations in soft-rays (Howard and Svestka, 1977) of interconnecting coronal loops suggest that loop coalescence may be a very important process for energy release in the solar corona. It was suggested (Tajima et al., 1982) that the most likely instability for impulsive energy release in solar flares is the coalescence instability (Tajima, 1982 ; Brunel et al., 1982). Tajima et al. (private communication) have examined the existing observational and theoretical results together with a global energy transfer model and have concluded that the merging of two current carrying solar loops can explain many of the known characteristics of solar flares, such as their impulsive nature, heating and high energy particle acceleration, amplitude oscillations of electromagnetic emission as well as the characteristics of microwave emission obtained during a flare. In particular, it was noted that the presence of strong electric fields and super-Alfvenic flows during the course of the instability play an important role in the production of non-thermal particles ; however, the relationship between both events and the mechanisms involved in the wave-particle interactions are still sources of open questions. As mentionned in Sect. IV, numerical simulation reveals to be a very powerful tool to approach this problem.

In complement to studies quoted in Secs. IV and V, an extensive study has been performed on the acceleration and heating of a very low β plasma by a strongly nonlinear magnetosonic wave (Lembège and Dawon, 1989b). Such a model has two advantages : (i) to follow how a nonlinear wave (sinusoïdal at time t=0, i.e. with a very narrow spectrum centered around a wave number k_o) may steepen into a shock profile (very large k-spectrum) in a strongly magnetized plasma ; (ii) to follow in details how both electrons and ions reach a relativistic regime for high values of ω_{ce}/ω_{pe}. For so doing, a 1-2/2D fully electromagnetic particles, relativistic code similar to that described in Sec. IV has been used, where the magnetosonic wave is excited by an external current with a phase velocity $\tilde{v}_\phi = \tilde{v}_A \equiv 0.5\,\tilde{c}$, where $\tilde{v}_A$ and $\tilde{c}$ are respectively the Alfven velocity and the light velocity ; the wave frequency $\tilde{\omega} = 0.14$ while gyrofrequencies are $\tilde{\omega}_{ce} = 3$ and $\tilde{\omega}_{ci} = 0.166$ respectively for electrons and ions.

In a first approach, the study has been restricted to a perpendicular propagation ($\vec{k} \perp \vec{B}_o$). In such a case , both particle species and fields exhibit a very rich dynamics and an highly nonlinear interaction which may be summarized as follow :

(a) since we have $v_\phi >> v_{the}$, electrons are strongly accelerated by the large electrostatic field and can reach relativistic velocity relatively shortly because of their light mass. Indeed, at large amplitude the wave requires very large transverse currents which are carried by the electrons ($\tilde{E} \times \tilde{B}$ drift) ; these can require electron velocities greater than $\tilde{v}_\phi$ in which case the electrons become relativistic. When this happens, a strong electron heating results. This feature greatly differs from the non-relativistic case ($\tilde{v}_\phi \cong \tilde{v}_{the}$) where electrons only exhibited a weak adiabatic compression heating (refs. of Sec. IV.1).

(b) Both fields $\tilde{E}_{lx}$ and $\tilde{E}_{ty}$ contribute to the ions acceleration until they become trapped, and detrapped at later times by the $\tilde{E} \times \tilde{B}$ drift . Since we are in a strongly magnetized plasma, the width of the trapping loop is very narrow ; ions are very energized by the $\tilde{E} \times \tilde{B}$ drift and succeed to reach a relativistic regime. Instead of forming a well collimated ring within the plane perpendicular to $\vec{B}_o$, as in the non-relativistic case, detrapped ions largely diffuse within a large area of the "light" circle ($\tilde{c} = 10$) . In addition, at early times the relation $\tilde{\omega} \cong \tilde{\omega}_{ci}$ is verified ; but during the build up phase of the wave, the $\tilde{B}_z$ field increases and $\tilde{\omega}$ becomes locally less than $\tilde{\omega}_{ci}$ at the wave maxima. At later times, relativistic effects become important (the relativistic factor $\tilde{\gamma}_i$ increases), and corrected ion gyrofrequency ($\omega_{ci} = qB / m_i \gamma_i$) decreases and forces to recover the resonance condition $\tilde{\omega} \cong \tilde{\omega}_{ci}$. Then, a very large ion heating results perpendicular to $\vec{B}_o$ by these two mechanisms : a large ion "diffuse" gyromotion and a "corrected" gyroresonance. Both effects lead to an important wave damping.

(c) Nonlinear effects and a phase shift between $\tilde{E}_{lx}$ and $\tilde{E}_{ty}$ fields are of central importance ; amplitude variations of these both fields strongly affect the dynamics of both electrons and ions but by a different way. Wave steepening appears with particle trapping and becomes noticeable after it : then, the initial sinusoïdal waveform evolves into a sawtooth. A ramp builds up in the wave profile similar to a shock : a large number of higher harmonics are generated in both electromagnetic and electrostatic components. A new event has been evidenced, for the first time to our knowledge, at later times of the run : solitary electron wavelets are emitted from the ramp, and may be explained as resulting from a balance between the wave steepening and dispersion effects. Indeed, the relativistic regime observed at later times is mainly characterized by spiky profiles of particles densities and of plasma

currents ; ion trapping observed in the relativistic regime drastically increases the wave steepening and hence the number of higher harmonics. Low k-modes mark one each other by propagating at a velocity which is dependant on its amplitude. When triggered with an amplitude large enough, they can easily pass the phase velocity $\tilde{v}_\phi$ of the input wave. Indeed the location of the ramp is associated with a very large local $\tilde{B}_z$ (much larger than $\tilde{B}_o$) and the local Alfven velocity may overcome $\tilde{v}_\phi$ ($\cong \tilde{v}_A$ at $\tilde{t}$ = 0). The high k-modes propagating more slowly (since $d\omega/dk < 0$ for $\theta = 90°$), lay the main waveform and promote the wavelets separation. Different solitary wavelets pass each other according to their relative velocity ; during their propagation, they locally accelerate electrons which largely diffuse within the "light" circle (Figure 14). This overall mechanism is the origin of a noticeable electron heating, which largely increases but stays less than ion heating ($\tilde{T}_e << \tilde{T}_i$).

(d) an extended parametric study was necessary in order to determine the efficiency of this mechanism according to the wave amplitude. Numerical results have stressed two possible regimes : for "small" wave amplitude, $\tilde{T}_e << \tilde{T}_i$, while $\tilde{T}_e >> \tilde{T}_i$, for "large" wave amplitude. The second regime corresponds to the formation of highly relativistic particles and may be explained as follows : the wave steepening is reinforced because of the initial larger amplitude, i.e. higher frequencies ($\tilde{\omega}_{st}$) modes are excited. On the other hand, the electron relativistic factor $\tilde{\gamma}_e$ becomes so large that the corrected gyrofrequency $\tilde{\omega}_{ce}$ drastically decreases until being of the order of the maximum frequency $\tilde{\omega}_{st}^{max}$, where subscript "st" holds as steepening. When this happens, a very important electron heating sets in by this "corrected" gyroresonance and leads to a strong increase of the temperature $\tilde{T}_e$.

Such results have been obtained for a finite "unrealistic" mass ratio ($m_i/m_e = 50$) in order to save computer time and to follow the dynamics of both particle species over a few ion gyroperiods. The striking feature is the particular efficiency of the mechanism as soon as it takes place. For large amplitude of the wave, the dynamics of ions nearly approaches that of electrons (a part of them gyrate and accumulate very nearly the "light" circle itself). These results illustrate how a sinusoidal waveform (here a magnetosonic wave) propagating within an electron-ion highly magnetized plasma tends towards the features of a relativistic wave propagating within an electron-positron plasma.

VII - PARTICLE SIMULATIONS ON NEW ARCHITECTURES OF HIGHLY PARALLEL COMPUTERS : AN APPLICATION TO A MAGNETOSPHERIC SHOCK

In the near future, parallel computers with terraflop performance will become available. The use of these machines will revolutionize computer simulations in many domains and in particular in studies of space plasma phenomena. Recently, Professor Dawson, in collaboration with Liewer, Decyk and Lembège, has used the 64-node Mark IIIfp hypercube parallel supercomputer to study electron dynamics in oblique magnetosonic shocks. The use of the parallel computers has allowed these shock studies to be extended into new parameter regimes which were previously computationally prohibitive (Liewer et al, 1991).

The foundations for these shocks studies on parallel computers was laid by Professor Dawson in about 1987 when he encouraged V. Decyk and P. Liewer to implement a 1-D electrostatic code on the 32-node Mark III hypercube parallel computer, then under construction at JPL. The 32-node Mark III, a predecessor of the Mark IIIfp, was significantly below Cray speed. However, Professor Dawson recognized the potential of these parallel computers at a time when most computational physicists were of the opinion that parallel computers were too difficult to program to ever be useful.

The recent concurrent simulations focused on the study of electron dynamics in quasi-perpendicular oblique shocks, e.g., shocks with a propagation angle relative to the shock normal in the range $\pi/2 - \sqrt{m_e/m_i} > \theta_{Bn} > \pi/4$. Such shocks are characterized by a standing whistler wavetrain preceding the shock (Tidman and Krall, 1971). It was found that linear and nonlinear interaction of the electrons with the precursor wave played an important role in these shocks. As mentionned in Sec. V.2, to study electron kinetic effects in shocks over long time scales, it is necessary to follow both the ion and electron dynamics, making such codes much more computationally intensive than hybrid code (fluid electrons-kinetic ions). The studies were carried out on the 64-processor Caltech/JPL Mark IIIfp hypercube concurrent supercomputer which provided the computational power to run this full particle code with realistic mass ratios ($m_i/m_e = 1600$) and extend the earlier studies of electron kinetic effects on shocks (Lembège and Dawson, 1987b, 1989a) into new parameter regimes.

Weak quasi-perpendicular oblique shocks have been observed in the Earth's bow shock under low β conditions (Greenstadt et al., 1975 ; Fairfield and Feldman, 1975 ; Mellott and Greenstadt, 1984). Detailed studies of such shocks by Mellott and Greenstadt (1984), using data from the ISEE 1 and 2 dual spacecraft mission, showed that the widths of these low Mach number laminar shocks scaled with the ion inertial length (c/ω_{pi}) as

expected theoretically for dispersive shocks ; no additional dissipation from cross-field streaming instabilities was necessary to explain the measured widths.

Both experimental (Feldman, 1975), and numerical studies (Lembège and Dawson, 1987b, 1989a) have emphasized that electrons may be accelerated along $\vec{B}_0$ in quasi-perpendicular oblique shocks under the effect of the parallel component of large electric fields. Analysis of ISEE 1 and 2 weak oblique shocks by Gary and Mellott (1985) indicated that electron damping of the whistler precursor wavetrain was important ; a self-consistent study of such effects also requires a kinetic treatment of electrons.

In the recent simulations of low Mach number ($M_A \leq 3$) oblique quasi-perpendicular shocks (Liewer and al, 1991), we found that electron dynamics play an important role in the shock structure. Specifically, we observe a strong interaction between the upstream electrons and the whistler precursor leading to a damping of the precursor and a heating of the electrons. In some parameter regimes, the electrons are seen to be trapped along the field lines in the electrostatic potential of the whistler, indicating significant nonlinear damping of the precursor. This can lead to strong electron heating in front of the shock when the parallel phase velocity of the whistler exceeds the electron thermal velocity.

A one-dimensional electromagnetic particle-in-cell code with kinetic electrons and ions was used for these studies, similar to that described in Lembège and Dawson [1987b]. The codes uses standard PIC techniques (Birdsall and Langdon, 1985) to solve the coupled equations for the particle orbits and the electromagnetic fields as an initial value problem. The parallel electromagnetic code was developped from a parallel electrostatic code implemented using the General Concurrent PIC algorithm described in Liewer and Decyk (1989). Run times for the studies in this paper range from four to fourteen hours.

Figure 15 shows results at two times in a simulation for a shock with $M_A = 2.8$ (determined from the observed propagation speed), $\beta_e = 0.02$, $\omega_{pe}/\omega_{ce} = 2$, $m_i/m_e = 1600$, $T_i/T_e = 4$, and $\theta_{Bn} = 70°$ (Case 1). Figures 15a-d show $B_z(x)$, electron v_x and v_z phase space, and $\phi(x)$ respectively at $t\omega_{pe} = 600$, and Figures 15e-h the same at $t\omega_{pe} = 1560$. Several features of the precursor wavetrain formation and electrons-precursor interaction in low Mach number oblique quasi-perpendicular shocks are illustrated in these series of plots.

The phase front of the wavetrain propagates faster than the shock, consistent with the observation of an increase in wave number in the packet with distance from the shock. Throughout this run, the wavetrain continued to extend farther from the shock, with new wave crests appearing, until the run was terminated when the system boundary was reached. Although the precursor wavetrain did not reach a "steady-state" shape in this run,

the amplitudes of the wavecrests nearer the shock front have reached steady-state amplitudes by the later time ($t\omega_{pe}$ = 1560).

The decrease in amplitude of the precursors with distance from the shock front indicated the presence of some convective damping mechanism. From the electron v_z versus x phase space plots in Figures 15c and 15g, it can be seen that the electron are interacting strongly with the precursor wavetrain (trapping in the electric potential), suggesting that electron damping may be present. Since v_z phase space is dominated by the electron motion parallel to the field for this θ_{Bn} = 70° case, the electrons are apparently interacting with the precursor via the parallel electric field of the precursor. Because the shock is propagating at an angle θ_{Bn} to the upstream magnetic field, there is a component of the shock and precursor electric fields parallel to the field :

$$E_{\parallel} = \nabla_{\parallel} \phi = \cos\theta_{Bn} \frac{d\phi}{dx}$$

To determine whether the potential is large enough to trap the electrons, the observed value of the potential well in the simulations can be compared to that required for trapping.

The phase velocity of the precursor parallel to the field is much higher than the velocity in the direction of propagation x, $v_{\phi//} = v_{\phi x} / \cos\theta_{Bn}$. Using $v_{\phi x} = M_A v_A$ for the standing precursor, the expression for the parallel phase velocity becomes $v_{\phi//} / v_{te} = M_A v_A / v_{te} \cos\theta_{Bn}$. For the run in Figure 15, the electron temperature was $T_e = 0.5\, T_e^0$, and Alven speed relative to the initial electron thermal speed was $v_A / v_{te} = 0.25$, yielding $v_{\phi//} / v_{te} \approx 2$.

For this simulation, the damping appears to be dominated by nonlinear (trapping) effects. However, if the run could be carried out for a longer time on a larger system so that a region of lower amplitude whistler were reached, a linear (Landau) damping region might also be observed.

If electron interaction with the parallel electric field of the precursor whistler is the cause of the electron heating and precursor damping as suggested by the simulation in Figure 15 (Case 1), then results should depend on the ratio of the precursor parallel phase velocity relative to the electron thermal velocity,

$$\frac{v_{\phi\parallel}}{v_{te}} = \frac{M_A v_A}{\cos\theta_{Bn} v_{te}} = \frac{M_A}{\cos\theta_{Bn}} \sqrt{\frac{2}{\beta_e} \frac{m_e}{m_i}} \qquad (15)$$

Figure 16, along with Figure 15e, shows results for the magnetic field at $t\omega_{pe} = 1560$ from three simulations with varying values of electron temperature, with other parameters the same as in Case 1 (Figure 15). Thus for Case 2, $v_{\phi//} / v_{te} \cong 1$, and for Case 3 $v_{\phi//} / v_{te} \cong 0.5$, compared to $v_{\phi//} / v_{te} \cong 2$ for Case 1.

Comparison of the precursor in the magnetic field in Figures 15 and 16 (Cases 1-3) shows that the decrease in $v_{\phi//} / v_{te}$, (from the increase in T_e), has lead to an increased convective damping of the whistler precursor. From these simulations results, we find that for $v_{\phi//} / v_{te} < 1$, the phase velocity lies well within the distribution and the electrons damp the precursor (linear damping) more than when $v_{\phi//} / v_{te} > 1$,. For $v_{\phi//} / v_{te} > 1$, the precursor causes more heating of the electrons as long as the precursor potential is large enough to trap a significant portion of the distribution function ; this leads to a non linear damping of the precursor.

The simulations here have shown that significant electron heating is observed when $v_{\phi//} / v_{te} > 1$. Using equation (15), the condition for a significant amount of electron heating can be written as :

$$\beta_e < 2 \frac{M_A^2}{\cos\theta_{Bn}} \frac{m_e}{m_i}$$

Thus for $m_i/m_e = 1836$ and $\cos\theta_{Bn} \cong 0.3$, $\beta_e < 0.01\, M_A^2$ is required . Thus the 1-D numerical simulations indicated that heating by the precursor whistler will be important in planetary and interplanetary shocks under low β_e conditions.

It is thus clear that details of electron dynamics are important for some shock structures, and thus simple fluid approximations are likely to miss important aspects of the physics. The calculations presented here have simply pointed up the richness of the physical phenomenon that can exist in plasma shocks. They cast light on only a small part of this and there are many questions left unanswered by these simple 1D electromagnetic calculations. In the future, as faster parallel supercomputers become available, and two-dimensional shock simulations on the electron time scale become practical, many more question about magnetosonic shocks will be answered.

VIII - CONCLUSIONS

We have given a synoptical review on some various topics and on innovative studies that Professor Dawson has carried out in numerical simulations of space plasma phenomena. Todays computers are able to follow the time evolution of systems containing many millions of degrees of freedom, all of which are simultaneously interacting with each other. One can often test theoretical predictions and the assumptions and approximations which go into them in ways inaccessible to laboratory or space experiments. For example, it is possible to turn effects on and off in such models and see how the results change. Needless to say, this is something which is often impossible in the real world.

On the other hand, such numerical tools are far more complete and realistic than we can hope to handle analytically. They reproduce both linear and nonlinear behavior. The results can be used to predict the behavior, test predictions and to gain an understanding of the phenomena involved. This aspect is particularly helpful for performing a comparative study with space experimental data and/or for the preparation of a new space project.

As mentionned by Professor Dawson (1981), "*the real power of numerical simulation does not lie (only) in reproducing complex physical phenomena. The results of such calculations often show us which are the important effects among the many possibilities and thus let us construct useful simple physical models which we would be hard pressed to justify a priori. Such calculations do not reduce the amount of physics we are called on to do, but rather increase the time spent on physics and put a premium on physical intuition*". "*On the experimental side, one is limited to measurements of only a small fraction of these quantities of interest in a process and even these may be only sampled at a few times and positions and with a limited degree of accuracy. This is particularly true for observations of natural phenomena such as are encountered with space plasmas*". We can add that, in many cases of large-scale and long-time natural phenomena, where observational studies are difficult or bring incomplete informations, such numerical approach represents an unique way for analysing in details the complexity of the phenomena and the simultaneous interaction of many effects.

Finally, let us remind that Professor Dawson also brought an important contribution in educating new researchers in the field of plasma simulation ; in particular, his active participation to successive International Simulation Schools of Space Plasmas illustrates quite well not only his deep interest in studying space plasma phenomena but also his care for establishing a link between fusion, space and astrophysics communities.

Figure captions

Figure 1. Global magnetospheric "substorm" simulation. These three insets show the evolution of the magnetospheric topology resulting from the passage over the magnetosphere of a rotational discontinuity which switches the solar wind field from east-west to southward.

Figure 2. Cold electron heating by loss cone instabilities. Perpendicular velocity distribution of the cold (blue) and hot (red) particles: their v_z-v_y phase space
a) at initial time,
b) at time of maximum wave amplitude,
c) in the nonlinear saturated state.

Figure 3. Ultrarelativistic sawtooth wave. Snapshots of the system at $\omega_{pe}t$= 120.
a) electrons p_x-x phase space;
b) electrons p_y-x phase space;
c) wave magnetic field B_z as a function of distance.

Figure 4. Numerical results illustrating the steepening of a large amplitude magnetosonic wave at time $\tilde{\tau}_{ci}$; $\tilde{E}_{lx}$ is the longitudinal electrostatic component ; $\tilde{E}_{ty}$ and $\tilde{B}_{tz}$ are the transverse electromagnetic components.Ion trapping loop clearly appears in plot (ii) ; electrons ($\tilde{p}_{xe}$, $\tilde{p}_{ye}$) only suffer an adiabatic compression heating.

Figure 5. Time history of ion temperatures $\tilde{T}_{xi}$ and $\tilde{T}_{yi}$ perpendicular to $\vec{B}_o$, and of field energies ; subscripts "l" and "t" hold respectively for longitudinal and transverse components. $\vec{B}_o$ is along z axis.

Figure 6. Three dimensional plot of the ion phase space at time $\tilde{t}$ = 1.8 $\tilde{\tau}_{ci}$ (i.e. after the ion trapping and detrapping have started) where $\tilde{\tau}_{ci}$ is the ion gyroperiod. The 3-D plot itself is in the central part of the picture where each point represents the position ($\tilde{p}_{xi}$, $\tilde{p}_{yi}$, $\tilde{x}$) of an ion. The three other plots represent the projections of the central plot on 2-D planes respectively ($\tilde{p}_{xi}$, $\tilde{x}$) , ($\tilde{p}_{yi}$, $\tilde{x}$) and ($\tilde{p}_{xi}$, $\tilde{p}_{yi}$) ; $\tilde{p}_{yi}$ and $\tilde{p}_{yi}$ are the momenta (≡ velocities) components. The arrow on the top indicates the direction of the wave propagation along x (from the bottom to the top of the figure) ; the dashed line is the phase velocity of the wave.

Figure 7. Plots of the maxima values of temperatures measured for ions (a) and electrons (b) along x, y and z direction. These values are deduced from plots of ion temperature

versus time obtained for each given angle θ ; $\vec{B}_o$ is along z for $\theta = 90°$ and is defined by $\vec{B}_o = (B_{ox}, O, B_{oz})$, for $\theta \neq 90°$.

Figure 8. Space profiles of the longitudinal field $\tilde{E}_{lx}$ and of the transverse fields $\tilde{E}_{ty}$ and $\tilde{B}_{tz}$ at different times ; P, O_1 and f indicate respectively the locations of the piston, of the first overshoot ,and of the magnetic foot.

Figure 9. Three dimensional plot of Log (f), where $f = f(\tilde{p}_{xi}, \tilde{p}_{yi})$ is the space-integrated ion distribution, and associated 2-D plot projections. Peaks P_1 and P_2 correspond, respectively to the unperturbed upstream ions, and to the compressed downstream (directly transmitted) ions. Ion ring is clearly apparent ; a second ring starts forming in the front part of the figure.

Figure 10. Plots of (a) the ion phase space $(\tilde{x}, \tilde{p}_{xi})$, (b) the electrostatic field $\tilde{E}_{lx}$, (c) the transverse electric field $\tilde{E}_{ty}$, (d) the magnetic field $\tilde{B}_{tz}$ and (e) and (f) the electron phase space $(\tilde{x}, \tilde{p}_{xe})$ and $(\tilde{x}, \tilde{p}_{ye})$. The dashed line in (a) represents the phase momentum of the wave $\tilde{p}_\phi \cong 1.8$; the arrows f, P, O_1, O_2 indicate, respectively, locations of the foot, of the piston, of the first and the second overshoot.

Figure 11. Electron phase space $(\tilde{x}, \tilde{p}_{\| e})$ for $\theta = 70°$ at various times $\tilde{t} = 0.14\ \tilde{\tau}_{ci}$ (a), $0.19\ \tilde{\tau}_{ci}$ (b), $0.28\ \tilde{\tau}_{ci}$ (c), and $0.38\ \tilde{\tau}_{ci}$ (d). Here, P and O_1 represent respectively the locations of the magnetic piston (where the particle density drops to zero), and of the first overshoot (maximum value of the magnetic field $\tilde{B}_z$ at the ramp).

Figure 12. Space profiles of field components and electrostatic potential for $\theta = 65°$ at various times of the run ; $\tilde{t} = 165$, 225 and 285 correspond respectively to $0.26\ \tilde{\tau}_{ci}$, $0.36\ \tilde{\tau}_{ci}$ and $0.45\ \tilde{\tau}_{ci}$.

Figure 13. Three dimensional plot of the ion phase space $(\tilde{x}_i, \tilde{v}_{xi}, \tilde{v}_{yi})$ (similar to that of Figure 6) in the case of a relativistic regime ; $\omega_{ce} / \omega_{pe} = 3$, $\tilde{c} = 10$ and $\vec{B}_o$ is along z axis.

Figure 14. Plots of the electron phase space $(\tilde{x}, \tilde{v}_{xe})$ and $(\tilde{x}, \tilde{v}_{ye})$ and velocity space $(\tilde{v}_{xe}, \tilde{v}_{ye})$ at different times $\tilde{t}$; the dashed line indicates the phase velocity of the wave ($\tilde{v}_\phi = 5.67$) ; the light velocity is c = 10 and $\vec{B}_o$ is along z axis.

Figure 15. Simulation results at two times from Case 1 for $\tilde{B}_z$ (normalized to $\sqrt{4\pi n_o m_e c^2}$), electron $(\tilde{x}, \tilde{v}_x)$ and $(\tilde{x}, \tilde{v}_z)$ phase space, and the electrostatic potential $\tilde{\phi}$ (normalized to T_e^0/e). This effect of the precursor wavetrain on the electrons can be seen in the phase space plots. For this case $v_{\phi//} / v_{te} \approx 2.0$. In 2d, the arrow shows the electron potential well of the first precursor. This precursor, as well as the smaller precursor, is large

enough to trap the entire electron distribution. In 2h, the arrow shows a finer scale secondary wave which appears to be associated with the trapped electrons.

Figure 16. Simulation results for $\tilde{B}_z$ for Cases 2 and 3, all at the same time as the later pictures in Figure 15 ($t\omega_{pe}$= 1560). Parameters are the same as Case 1 (Figure 15), except ($v_{\phi//}$/ v_{te} = 1.0) for Case 2 and ($v_{\phi//}$/ v_{te} = 0.4) for Case 3. More convective damping of the precursor wavetrain is evident in the warmer case, Case 3. M_A= 2.8 for Cases 1-3.

REFERENCES

1. Ashour-Abdalla, N., J. N. Leboeuf, J. M. Dawson, and C. F. Kennel, "A simulation study of cold electron heating by loss cone instabilities", *Geophys. Res. Lett. 7*, 889, 1980.

2. Ashour-Abdalla, M., J. N. Leboeuf, T. Tajima, C. F. Kennel, and J. M. Dawson, "Ultrarelativistic electromagnetic pulses in plasmas", *Phys. Rev. A23*, 1906, 1981.

3. Ashour-Abdalla, N., J. N. Leboeuf, J. M. Dawson, and C. F. Kennel, "A simulation study of cold electron heating by loss cone instabilities", *Geophys. Res. Lett. 7*, 889, 1980.

4. Birdsall, C.K., and Langdon, A.B., "Plasma physics via computer simulation", McGraw-hill, New York, 1985.

5. Biskamp, D., "Collisionless shock waves in plasma", *Nuclear Fus., 13*, 719-740, 1973.

6. Biskamp, D. and H. Welter, "Numerical studies of magnetosonic collisionless shock waves" ,*Nuclear Fus., 12*, 663 , 1973.

7. Brunel, F. , J. N. Leboeuf, T. Tajima, J. M. Dawson, M. Makino, and T. Kamimura, "Magnetohydrodynamic particle code: Lax-Wendroff algorithm with finer grid interpolations", *Journ. Comp. Phys. 43*, 268, 1981.

8. Brunel F., T. Tajima and J.M. Dawson,,*Phys. Rev. Lett., 49*, 323, 1982.

9. Burgess, D., "Numerical simulation of collisionless shocks", in Proceedings of International Conference on Collisionless shocks, Bulatonfured, Hungary, pp. 89-111, ed. by Szego, 1987.

10. Dawson, J.M., "Simulations of space plasma phenomena", in Physics of Auroral Arc Formation", *Geophys. Monograph Series*, 25, 1981.

11. Dawson, J.M., V. K. Decyk, R. W. Huff, I. Jechart, T. Katsouleas, J. N. Leboeuf, B. Lembege, R. M. Martinez, Y. Ohsawa, and S. T. Ratliff, " Damping of large amplitude plasma waves propagating perpendicular to the magnetic field", *Phys. Rev. Lett. 50*, 1455, 1983.

12. Décréau ,P.M.E., C. Béghin and M. Parrot, "Global characteristics of the cold plasma in the equatorial plasmapause region as deduced from the GEOS 1 mutual impedance probe", *J. Geophys. Res.*, 87, 695, 1982.

13. Dungey, J. W. , "Interplanetary magnetic field and the auroral zones", *Phys. Rev. Lett. 6*, 47, 1961.

14. Fairfield, D.H. and W.C. Feldman, "Standing waves at low Mach number laminar bow shocks", *J. Geophys. Res., 80*, 515, 1975

15. Feldman, W.C., "Electron velocity distributions near collisionless shocks", in *Collisionless Shocks in the Heliosphere : Reviews of Current Research* (B. Tsurutani and R.G. Stone ,eds, AGU, Washington D.C.) p. 195, 1985.

16. Gary, S.P. and M.M. Mellott, "Whistler damping at oblique propagation : laminar shock precursors", *J. Geophys. Res., 90*, 99, 1985.

17. Gendrin, R., "Consequences of hydromagnetic waves on magnetospheric particle dynamics", *Space Science Rev.* 42, 515, 1985.

18. Goodrich, C.C., "Numerical simulations of quasi-perpendicular collisionless shocks", in *Collisionless Schocks in the Heliosphere* : Review of Current Research, Geophys. Monograph. Ser., Vol. 35, pp. 153-168, ed. by B.T. Tsurutani and R.G. Stone, AGU Washington, D.C., 1985.

19. Greenstadt, E.W., C.T. Russel, F.L. Scarf, V. Formisano, and M. Neugebauer, "Structure of the quasi-perpendicular laminar bow shock", *J. Geophys. Res., 80*, 502, 1975.

20. Gurnett, D.A., F.L. Scarf, R.W. Fredricks and E.J. Smith, "The ISEE-1 and ISEE-2 plasma investigation", *Geoscience Electronics GE-16*, 225, 1978.

21. Hones, E. W. , Jr., D. N. Baker, S. J. Bame, W. C. Feldman, J. T. Gosling, D. J. Mc Comas, R. D. Zwickl, J. A. Slavin, E. J. Smith, and B. Tsurutani, " Structure of the magetotail at 220 RE and its response to geomagnetic activity", *Geophys. Res. Lett. 11*,5, 1984.

22. Howard, R. and Z. Svestka, *Solar Phys.*, 54, 65, 1977.

23. Katsouleas, T. and J. M. Dawson, " Unlimited electron acceleration in laser driven plasma waves", *Phys. Rev. Lett. 51*, 392, 1983.

24. Kennel, C. F. , F. S. Fujimura, and R. Pellat, *Space Sci. Rev. 24*, 407, 1979.

25. Kennel, C.F., Edminston, J.P. and T. Hada, "A quarter century of collionless shock research", in *Collisionless Schocks in the Heliosphere* : Reviews of Current Research, Geophys. Monograph. Ser., Vol. 35, pp. 1-36, ed. by B.T. Tsurutani and R.G. Stone, AGU Washington, D.C., 1985.

26. Korth, A., G. Kremser, A. Roux, S. Perraut, J.A. Sauvaud, J.M. Bosqued, A. Pedersen and B. Aparicio, "Drift boundaries and ULF wave generation near noon at geostationary orbit", *Geophys. Res. Lett., 10*, 639, 1983.

27. Korth, A., G. Kremser, S. Perraut, and A. Roux, "Interaction of particles with ion cyclotron waves and magnetosonic waves. Observations from GEOS 1 and 2", *Planet. Space Sci., 32*, 1393, 1984.

28. Kurth, W. S. , L. A. Frank, M. Ashour-Abdalla, D. A. Gurnett, and B. G. Burek, "A free energy source for intense electrostatic waves", *Geophys. Res. Lett. 7*, 293, 1980.

29. Leboeuf., J. N. L, T. Tajima, C. F. Kennel, and J. M. Dawson, "Global simulation of the time-dependent magnetosphere", *Geophys. Res. Lett 5*, 609, 1978.

30. Leboeuf, J. N. , T. Tajima, and J. M. Dawson, "A magnetohydrodynamic particle code for fluid simulations of plasmas", *Journ. Comp. Phys. 31*, 379, 1979.

31. Leboeuf, J. N., T. Tajima, C. F. Kennel, and J. M. Dawson, "Global magneto-hydrodynamic simulation of the two-dimensional magnetosphere", in Quantitative Modeling of Magnetospheric Processes, *Geophysical Monograph 21*, edited by W. P. Olson, American Goephysical Union, Washington, D. C., 1979.

32. Leboeuf, J. N. , T. Tajima, C. F. Kennel, and J. M. Dawson, "Global simulations of the three-dimensional magnetosphere", *Geophys. Res. Lett. 8*, 257, 1981.

33. Leboeuf, J. N., M. Ashour-Abdalla, T. Tajima, C. F. Kennel, F. V. Coroniti, and J. M. Dawson, " Ultrarelativistic waves in overdense electron-positron plasmas", *Phys. Rev. A*, 25, 1023, 1982.

34. Lembège, B. , S. T. Ratliff, J. M. Dawson, and Y. Ohsawa, " Ion heating and acceleration by strong magnetosonic waves", *Phys. Rev. Lett. 51*, 264, 1983.

35. Lembège, B. ,and J.M. Dawson, "Plasma heating and acceleration by strong magnetosonic waves propagating obliquely to a magnetostatic field", *Phys. Rev. Lett. 53*, 11, 1053, 1984a.

36. Lembège , B., and J.M. Dawson , "Kinetic perpendicular collisionless shocks". *UCLA Report*, PPG-832, 1984b.

37. Lembège, B, and J.M. Dawson, "Self-consistent study of a perpendicular collisionless and nonresistive shocks", *Phys. Fluids 30*(6), 1767, 1987 a.

38. Lembège, B., and J.M. Dawson, "Plasma heating through a supercritical oblique collisionless shock" , *Phys. Fluids 30* (4), 1110, 1987 b.

39. Lembège, B., and J.M. Dawson, "Formation of double layers within an oblique collisionless shock",*Phys. Rev. Lett. 62* (23), 2683, 1989 a.

40. Lembège, B. and J. M. Dawson, "Relativistic particle dynamics in a steepening magnetosonic wave", *Phys. Fluids B1*, 1001, 1989b.

41. Lembège, B. and J. M. Dawson, " Self consistent plasma heating and acceleration by strong magnetosonic waves for $\theta = 90^{o}$. Part I: basic mechanisms", *Phys. Fluids 29*, 3, 821, 1986.

42. Leroy, M.M., C.C. Goodrich, D. Winske, C.S. Wu and K. Papadopulos, "Simulation of a perpendicular bow shock". *Geophys. Res. Lett. 8*, 1269 ,1981.

43. Leroy, M.M., D. Winscke, C.C. Goodrich, C.S. Wu and K. Papadopoulos, "The structure of perpendicular bow shocks". *J. Geophys. Res. Lett, 87*, 5081, 1982.

44. Liewer, P.C., and V.K. Decyk, "A general conurrent algorithm for plasma particle-in-cell simualtion codes", J. *Comp. Physics, 85*, 302, 1989.

45. Liewer P.C., V.K. Decyk, J.M. Dawson and B. Lembège, "Numerical studies of electron dynamics in oblique quasi-perpendicular collisionless shock waves", *J. Geophys. Res.*, (in press) 1991.

46. Mellott, MM., and E. W. Greenstadt, "The structure of oblique subcritical bow shocks : ISEE1 and 2 observations", *J. Geophys. Res. 89*, 2151, 1984.

47. Papadopoulos, K., "Microinstabilities and anomalous transport", in *Collisionless Shocks in the Heliosphere* : Review of Current Research, Geophys. Monograph. Ser., Vol. 35, pp. 59-88, ed. by B.T. Tsurutani and R.G. Stone, AGU Washingtn, D.C., 1985.

48. Perraut, S., A. Roux, P. Robert, R. Gendrin, J.A. Sauvaud, J.M. Bosqued, G. Kremser and A. Korth, "A systematic study of ULF waves above f_H^+ from GEOS 1 and 2 mesurements and their relationships with proton ring distributions", *J. Geophys. Res. 87*, 6219, 1982.

49. Podgorny, I. M. , E. M. Dubinin, P. L. Izrailevich, Y. N. Potanin, " Plasma dynamics in laboratory models of the magnetosphere of the Earth and Uranus", *Izv. An. Ser. Fiz. 41*, 1870, 1977.

50. Quest, K.B., "Simulations of high Mach number collisionless perpendicular shocks in astrophysical plasmas", *Phys. Rev. Lett.*, 54, 1872-1874, 1985.

51. Quest, K.B., "Simulations of high Mach number perpendicular shocks with resistive electrons". *J. Geophys. Res. 91*, 8805, 1986.

52. Quest, K.B., "Hybrid simulation" in Numerical Simulation of Space Plasmas, Proceedings of ISSS-3, Part 1, p.177-182, *Cepadues Editions*, Toulouse France (1989).

53. Sagdeev, R.Z., "The 1976 Oppenheimer lectures : critical problems in plasma astrophysics, II, Singular layers and reconnection", *Rev. Mod. Phys., 51*, 11, 1979.

54. Sentman, D. D. , J. N. Leboeuf, T. Katsouleas, R. W. Huff, and J. M. Dawson, "Electrostatic instabilities of velocity-space-shell distributions in magnetized plasmas", *Phys. Fluids 29*, 2569, 1986.

55. Tajima, T. and J. M. Dawson, *Phys. Rev. Lett.* 43, 267, 1979.

56. Tajima, T., F. Brunel and J.I. Sakai, "Loop coalescece in flares and coronal X-ray brightening", *The Astrophys. J. , 258*, L45, 1982.

57. Tajima, T., in "Fusion Energy", *International Atomic Energy Agency, ICTP*, Trieste, 403, 1982.

58. Tajima, T., F. Brunel, J. I. Sakai, Toyama, L. Vlahos and M.R. Kundu, "The coalescence instability of solar flares", (*private communication*).

59. Tidman, D.A. and N.A. Krall", Shock waves in collisionless plasma", Wiley, *Interscience*, New York, 1971)

60. Winske, D. and M.M. Leroy, "Hybrid simulation techniques applied to the Earth's low shock", in *Computer Simulation of Space Plasmas*, ISSS-1, ed. by Matsumoto and T. Sato, pp. 255-278, Kluwer Academic, Hingham, Mass 1984.

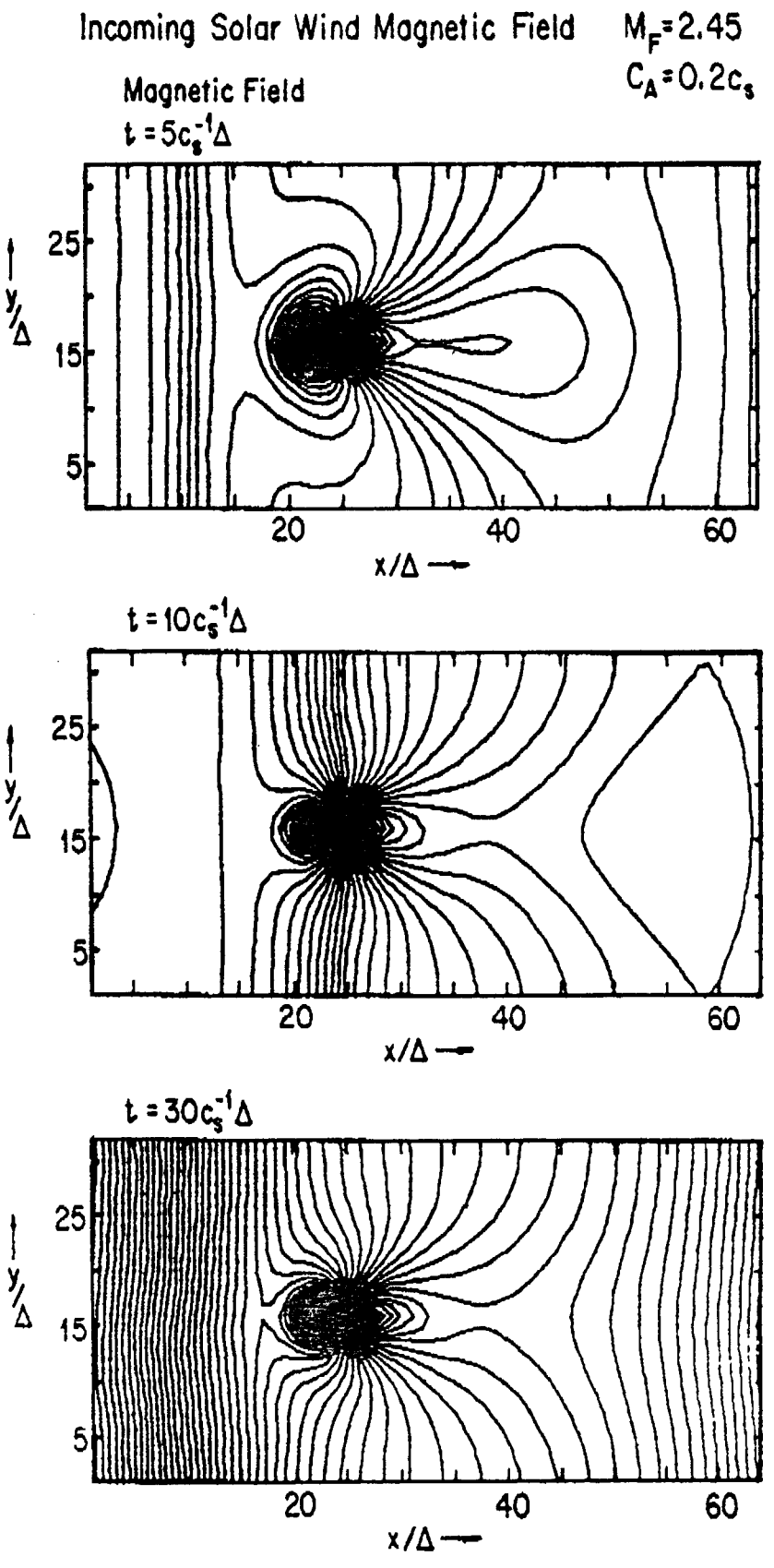
Incoming Solar Wind Magnetic Field
$M_F = 2.45$
$C_A = 0.2c_s$
Magnetic Field
$t = 5c_s^{-1}\Delta$
$t = 10c_s^{-1}\Delta$
$t = 30c_s^{-1}\Delta$
y/Δ
x/Δ
5
15
25
20
40
60

Figure 1

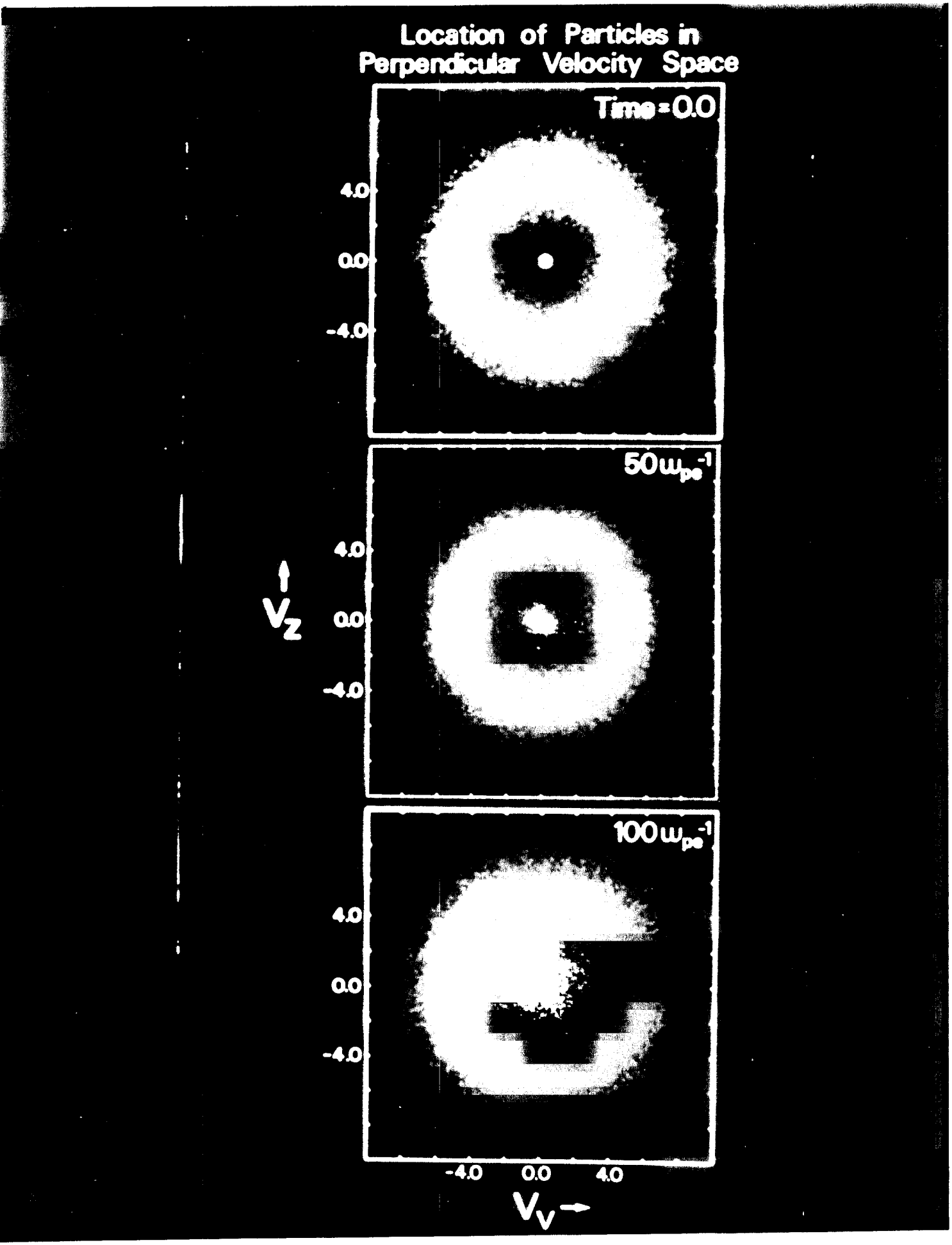
Location of Particles in
Perpendicular Velocity Space
Time=0.0
4.0
0.0
-4.0
50 ω_{pe}^{-1}
4.0
0.0
-4.0
V_z
100 ω_{pe}^{-1}
4.0
0.0
-4.0
-4.0
0.0
4.0
V_v

Figure 2

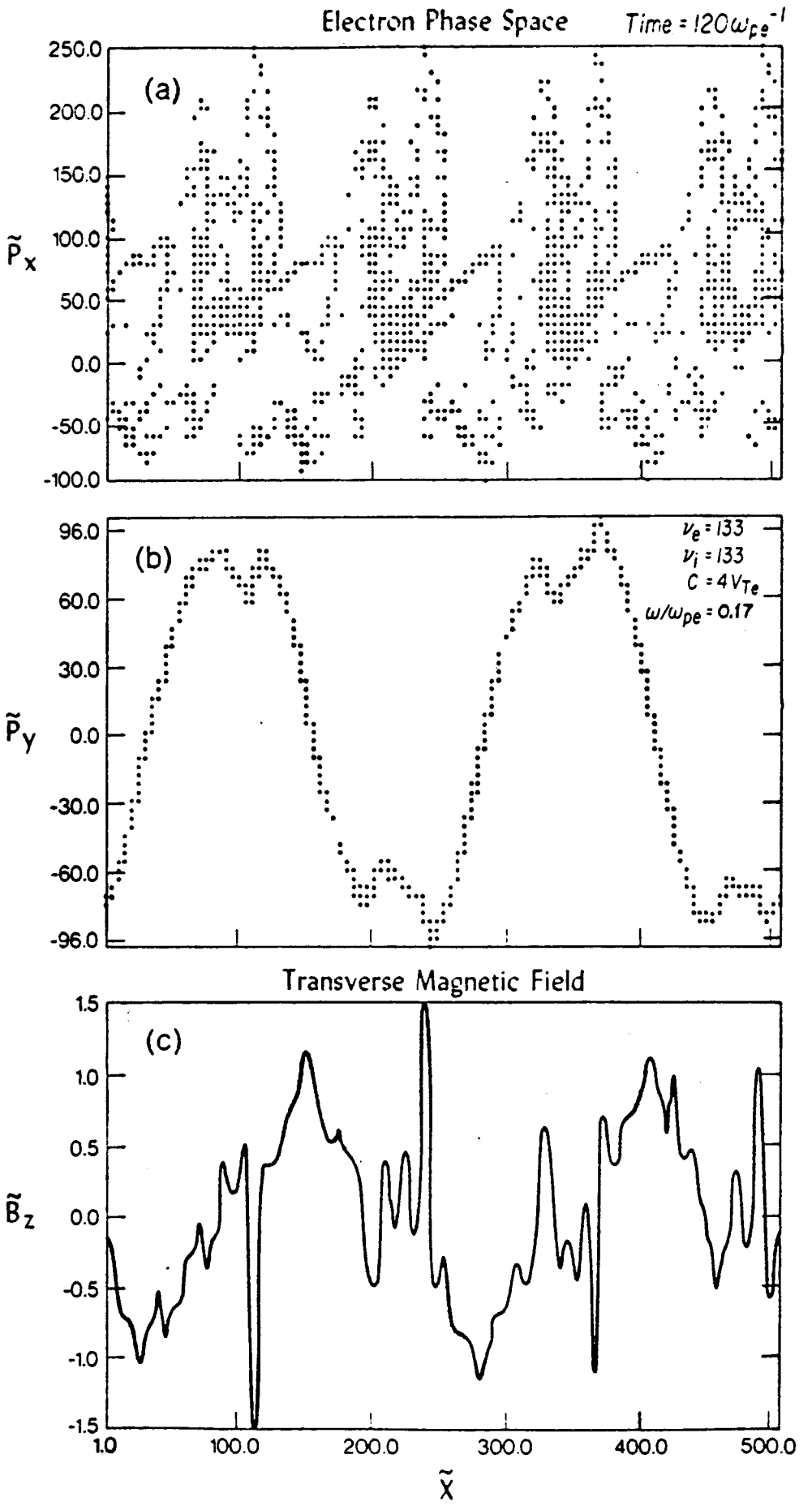
Electron Phase Space
Time = 120 ω_{pe}^{-1}
(a)
250.0
200.0
150.0
100.0
50.0
0.0
-50.0
-100.0
$\tilde{P}_x$
(b)
$\nu_e = 133$
$\nu_i = 133$
$C = 4 V_{Te}$
$\omega/\omega_{pe} = 0.17$
96.0
60.0
30.0
0.0
-30.0
-60.0
-96.0
$\tilde{P}_y$
Transverse Magnetic Field
(c)
1.5
1.0
0.5
0.0
-0.5
-1.0
-1.5
$\tilde{B}_z$
1.0
100.0
200.0
300.0
400.0
500.0
$\tilde{X}$

Figure 3

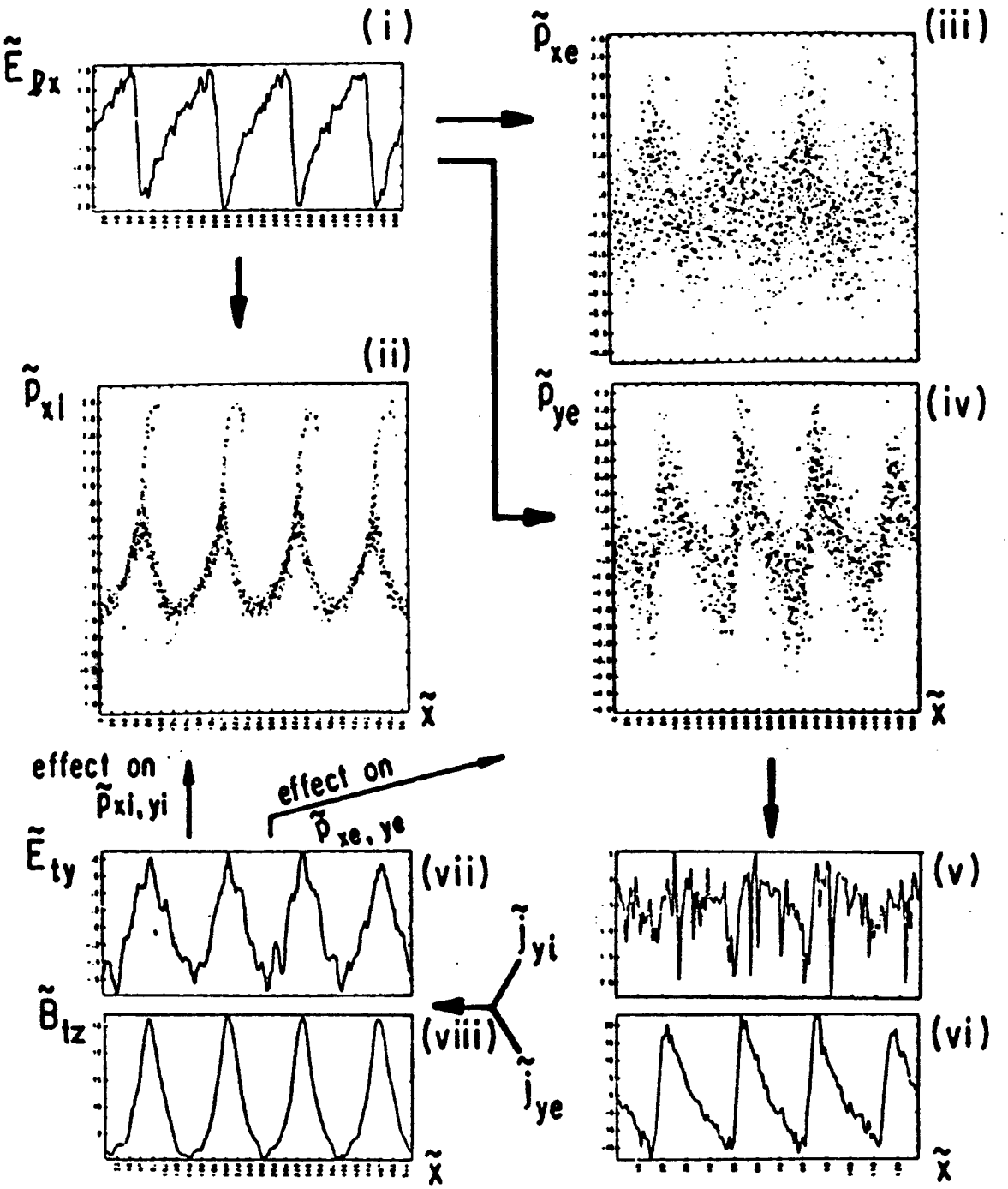
(i)
$\tilde{E}_{gx}$
(ii)
$\tilde{p}_{xi}$
$\tilde{x}$
(iii)
$\tilde{p}_{xe}$
(iv)
$\tilde{p}_{ye}$
$\tilde{x}$
effect on $\tilde{p}_{xi,yi}$
effect on $\tilde{p}_{xe,ye}$
$\tilde{E}_{ty}$
(vii)
$\tilde{B}_{tz}$
(viii)
$\tilde{j}_{yi}$
$\tilde{j}_{ye}$
$\tilde{x}$
(v)
(vi)
$\tilde{x}$

Figure 4

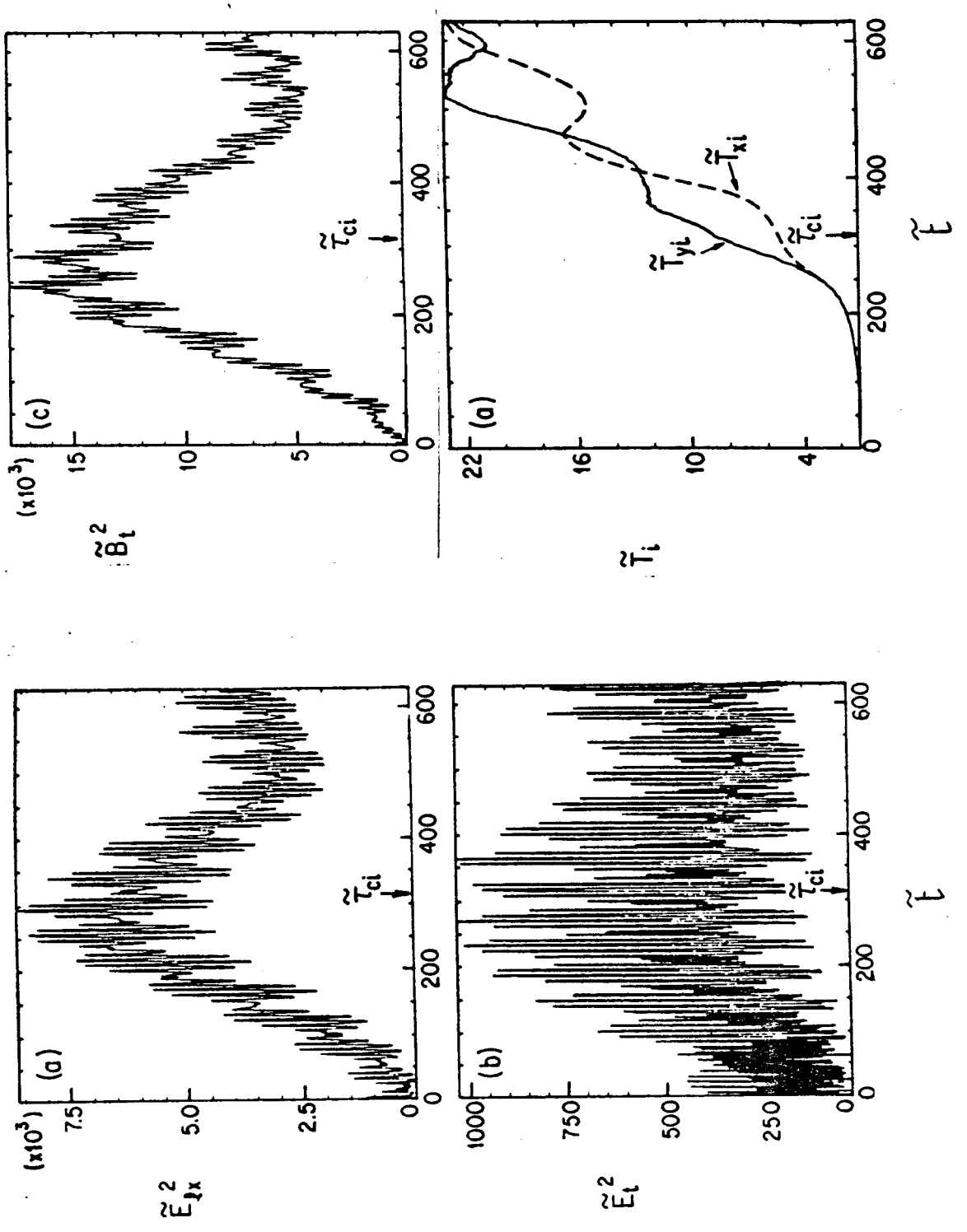
(a)
(b)
(c)
(a)
$\tilde{E}_{tx}^2$
$\tilde{E}_t^2$
$\tilde{B}_t^2$
$\tilde{T}_i$
$\tilde{T}_{ci}$
$\tilde{T}_{xi}$
$\tilde{T}_{yi}$
$\tilde{t}$
(x10^3)
0
200
400
600
2.5
5.0
7.5
250
500
750
1000
4
10
16
22
5
10
15

Figure 5

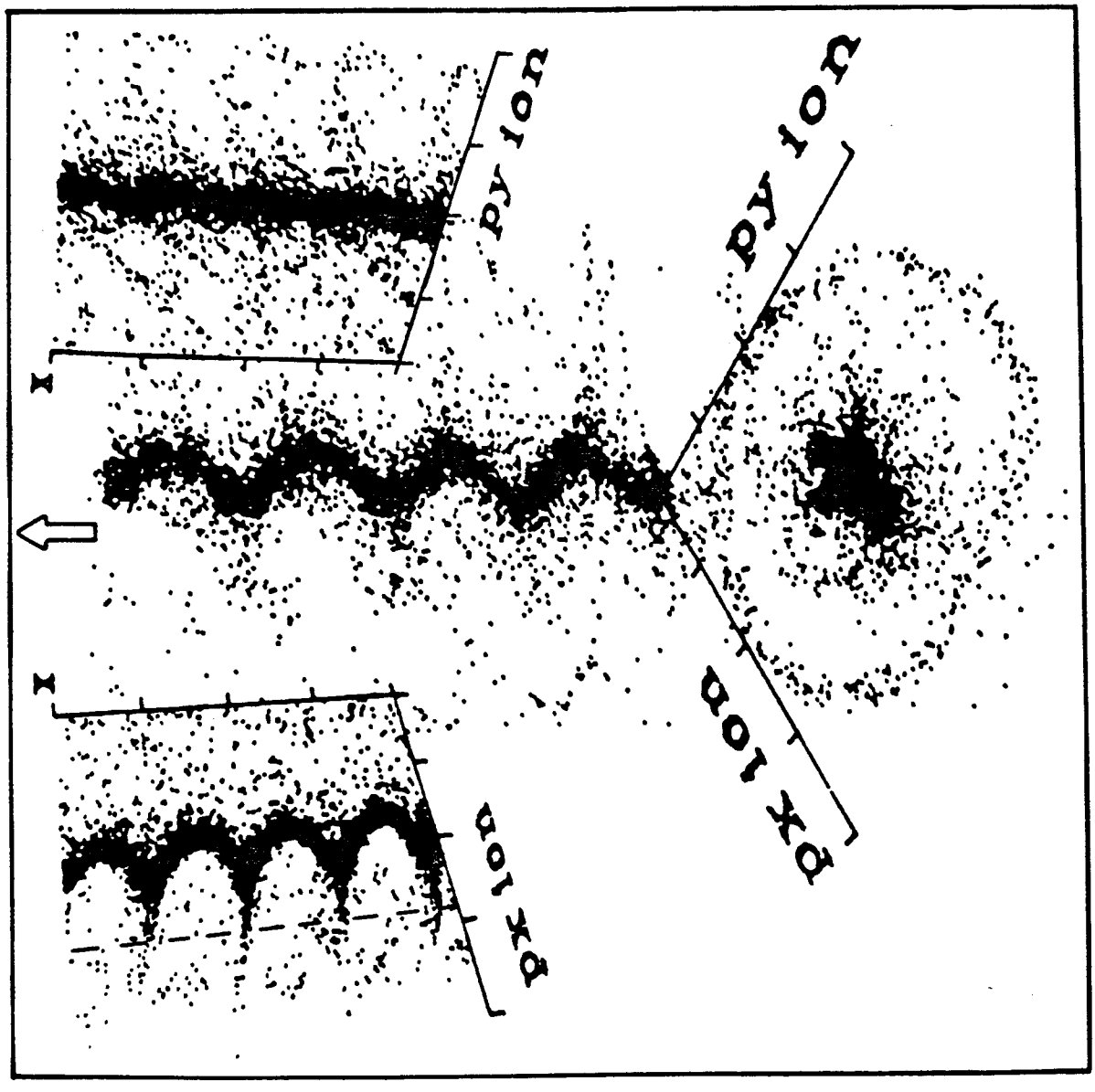

Figure 6

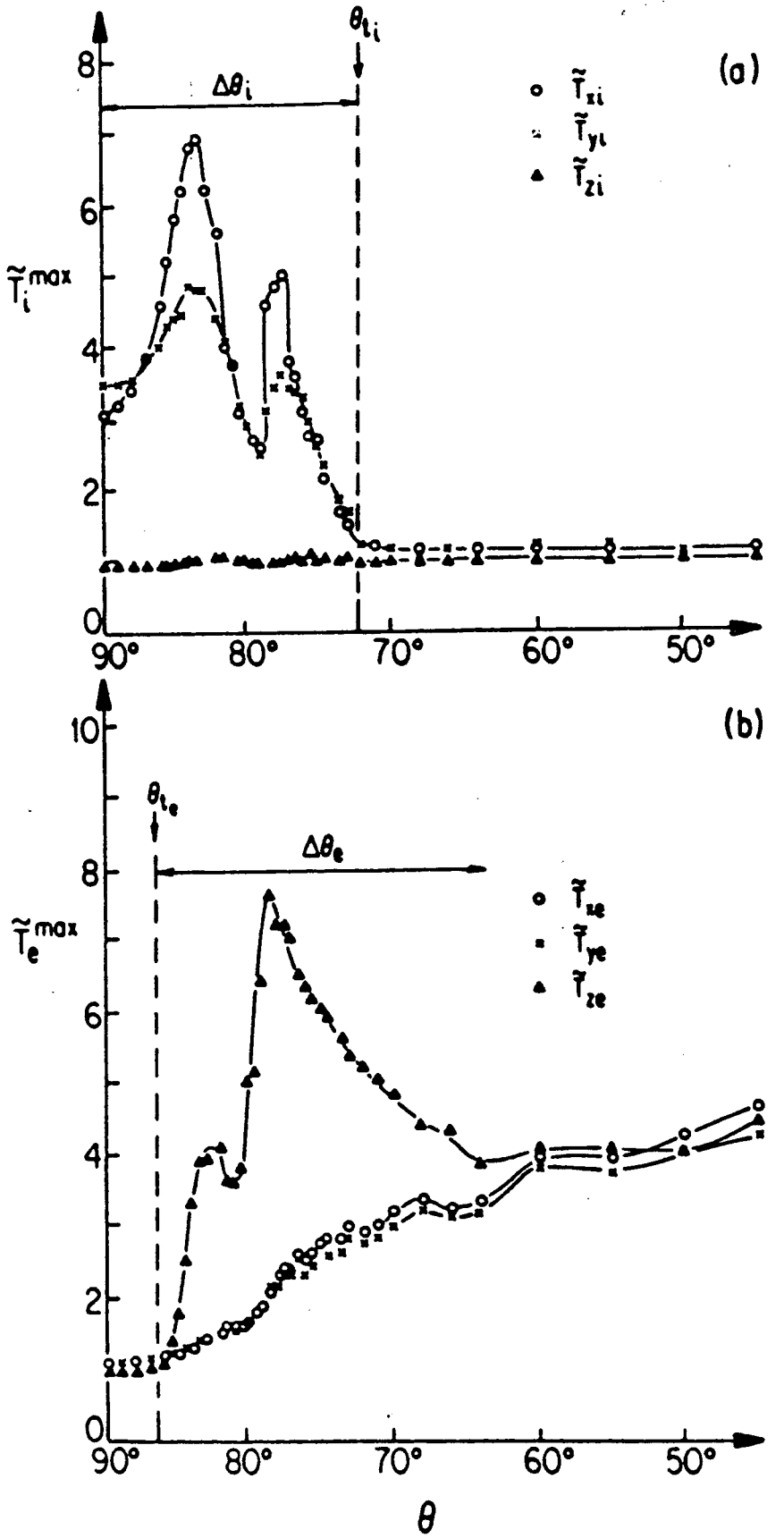
(a)
θ_{ti}
$\Delta\theta_i$
$\tilde{T}_{xi}$
$\tilde{T}_{yi}$
$\tilde{T}_{zi}$
$\tilde{T}_i^{max}$
8
6
4
2
0
90°
80°
70°
60°
50°
(b)
θ_{te}
$\Delta\theta_e$
$\tilde{T}_{xe}$
$\tilde{T}_{ye}$
$\tilde{T}_{ze}$
$\tilde{T}_e^{max}$
10
8
6
4
2
0
90°
80°
70°
60°
50°
θ

Figure 7

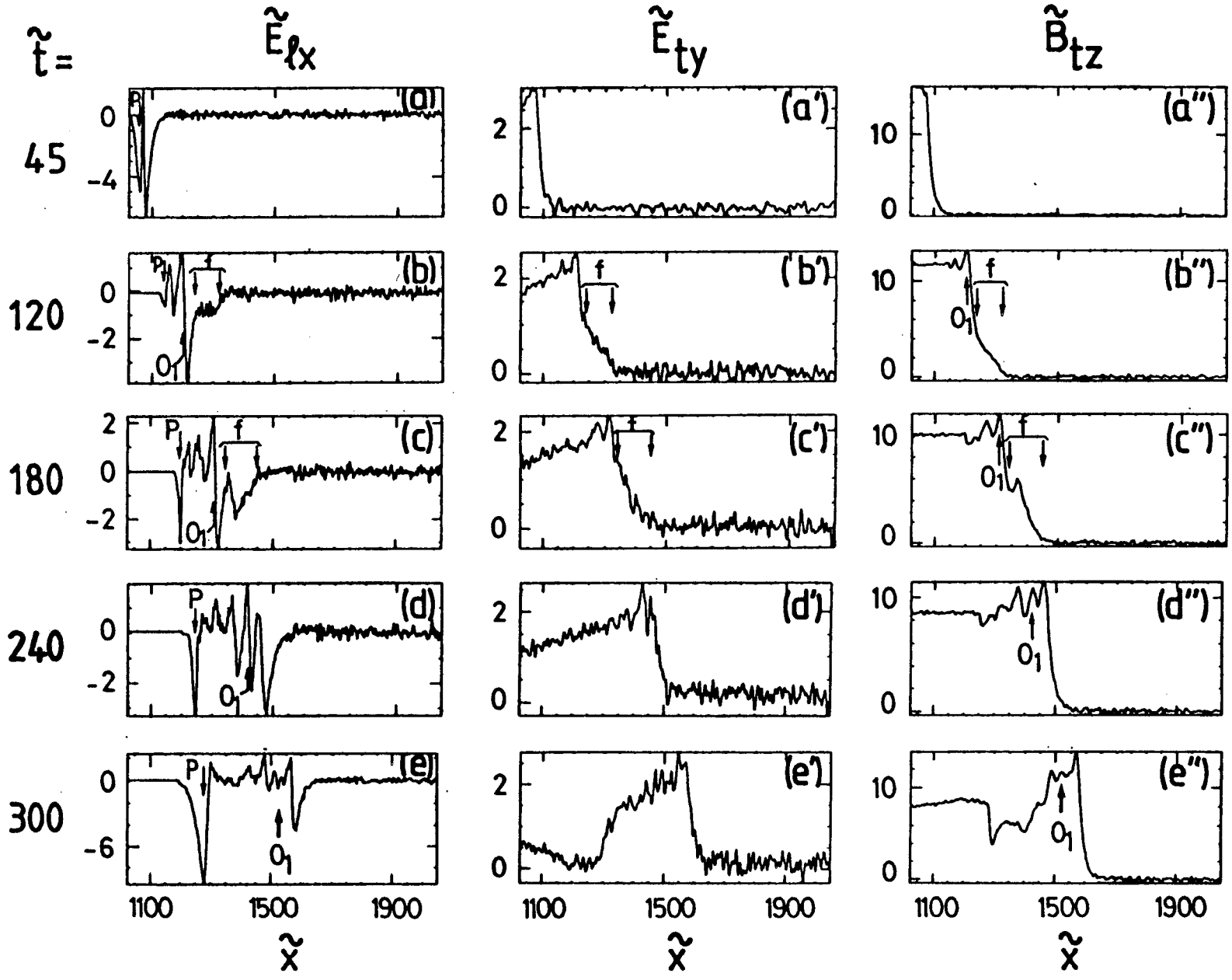
$\tilde{t}$=
$\tilde{E}_{\ell x}$
$\tilde{E}_{ty}$
$\tilde{B}_{tz}$
45
120
180
240
300
(a)
(a')
(a'')
(b)
(b')
(b'')
(c)
(c')
(c'')
(d)
(d')
(d'')
(e)
(e')
(e'')
P
f
O_1
0
-4
2
10
-2
-6
1100
1500
1900
$\tilde{x}$

Figure 8

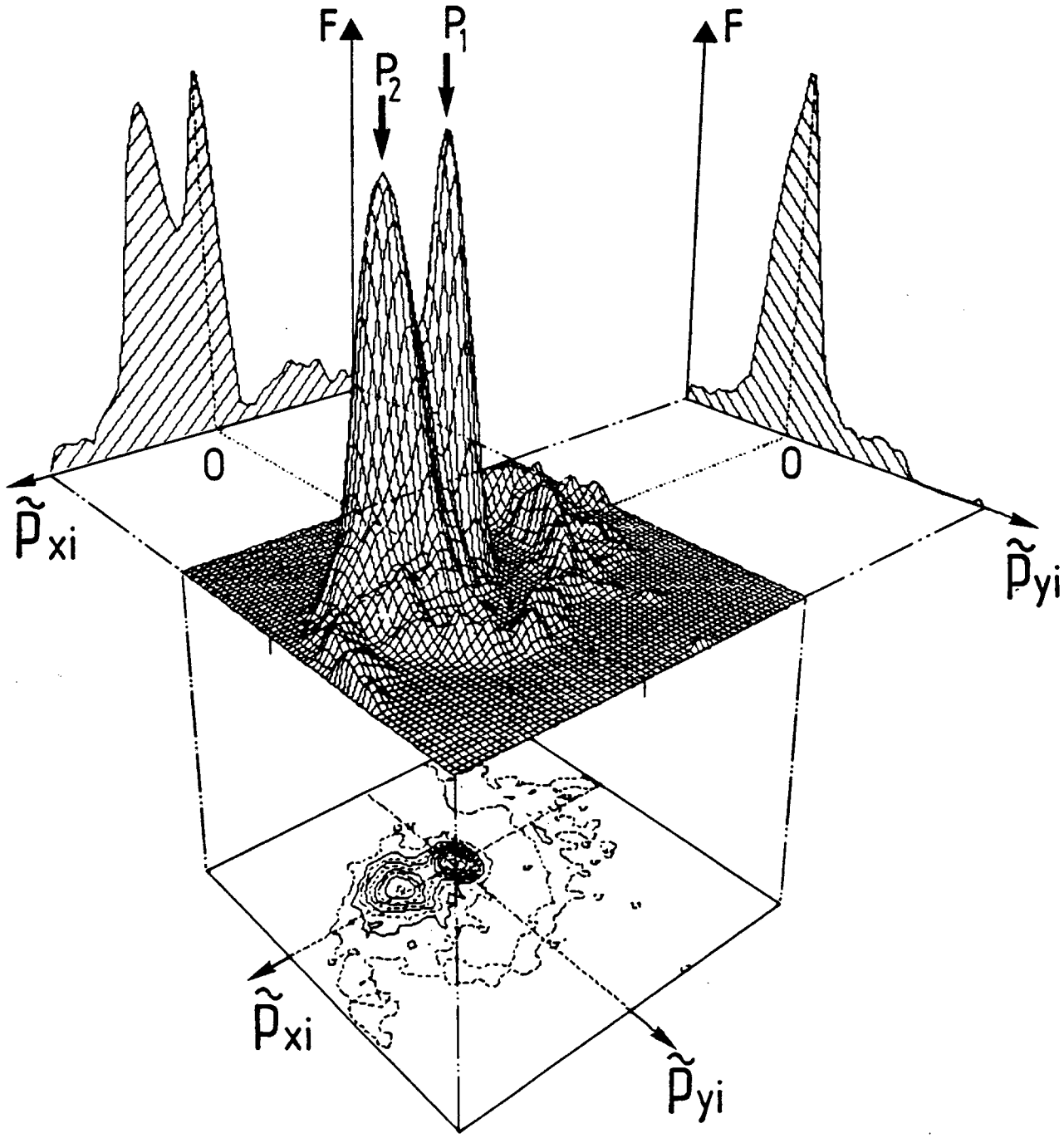

Figure 9

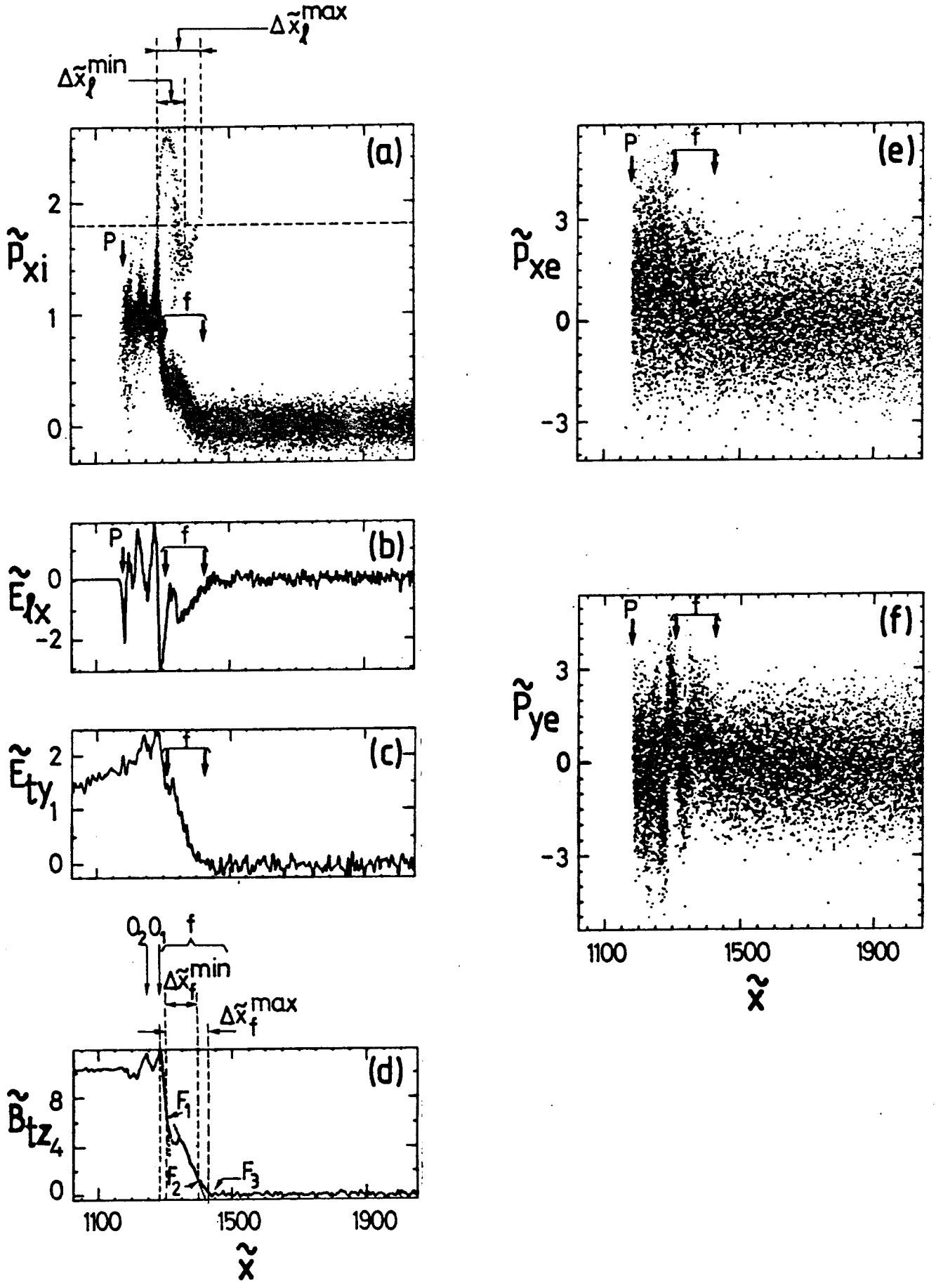
(a)
(b)
(c)
(d)
(e)
(f)
P
f
$\Delta\tilde{x}_\ell^{max}$
$\Delta\tilde{x}_\ell^{min}$
$\tilde{P}_{xi}$
$\tilde{E}_{\ell x}$
$\tilde{E}_{ty_1}$
$\tilde{B}_{tz_4}$
$\tilde{P}_{xe}$
$\tilde{P}_{ye}$
O_2 O_1
$\Delta\tilde{x}_f^{min}$
$\Delta\tilde{x}_f^{max}$
F_1
F_2
F_3
1100
1500
1900
$\tilde{x}$

Figure 10

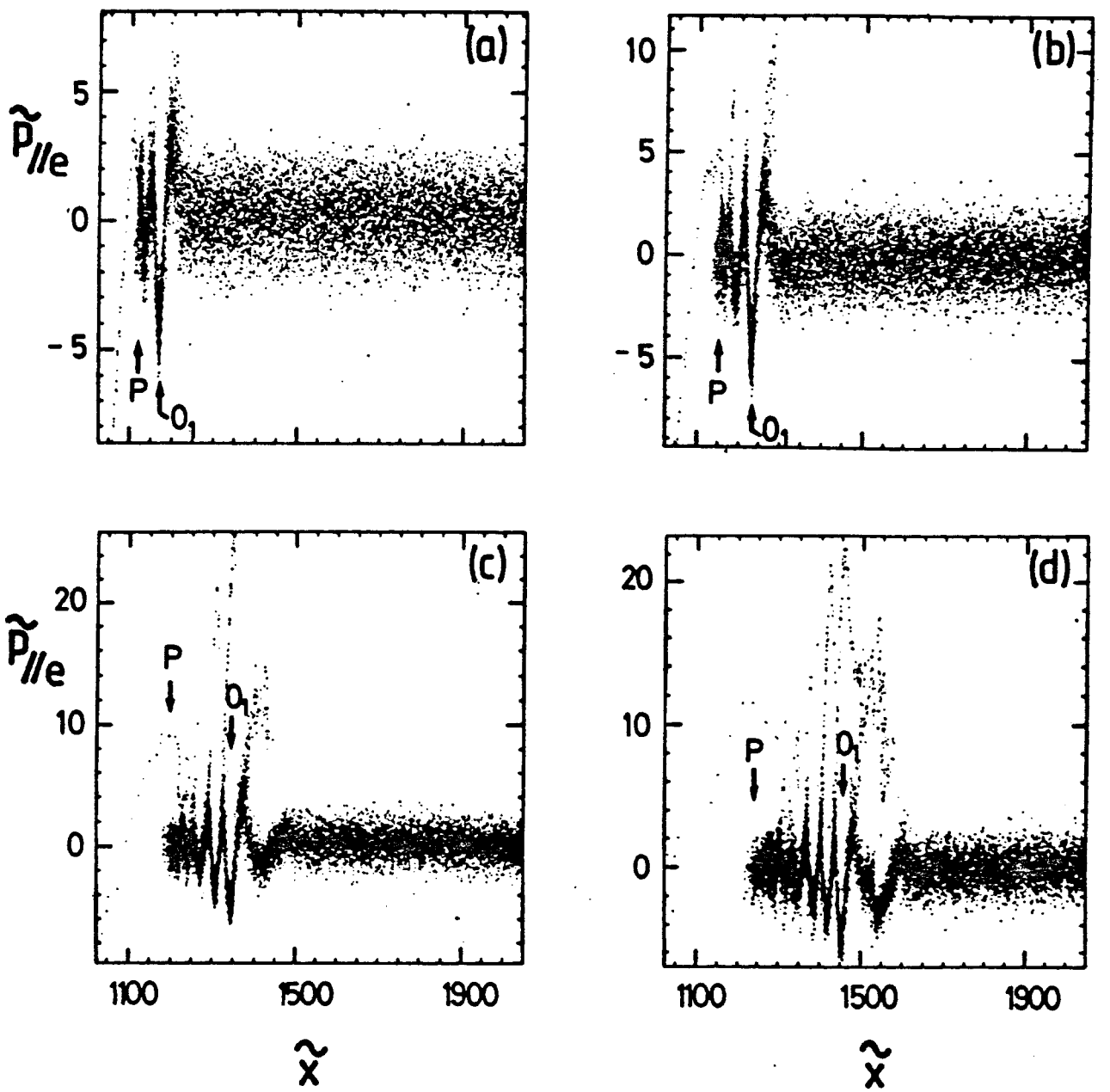
(a)
(b)
(c)
(d)
$\tilde{P}_{//e}$
$\tilde{P}_{//e}$
5
0
-5
10
5
0
-5
20
10
0
20
10
0
P
O_1
1100
1500
1900
$\tilde{x}$

Figure 11

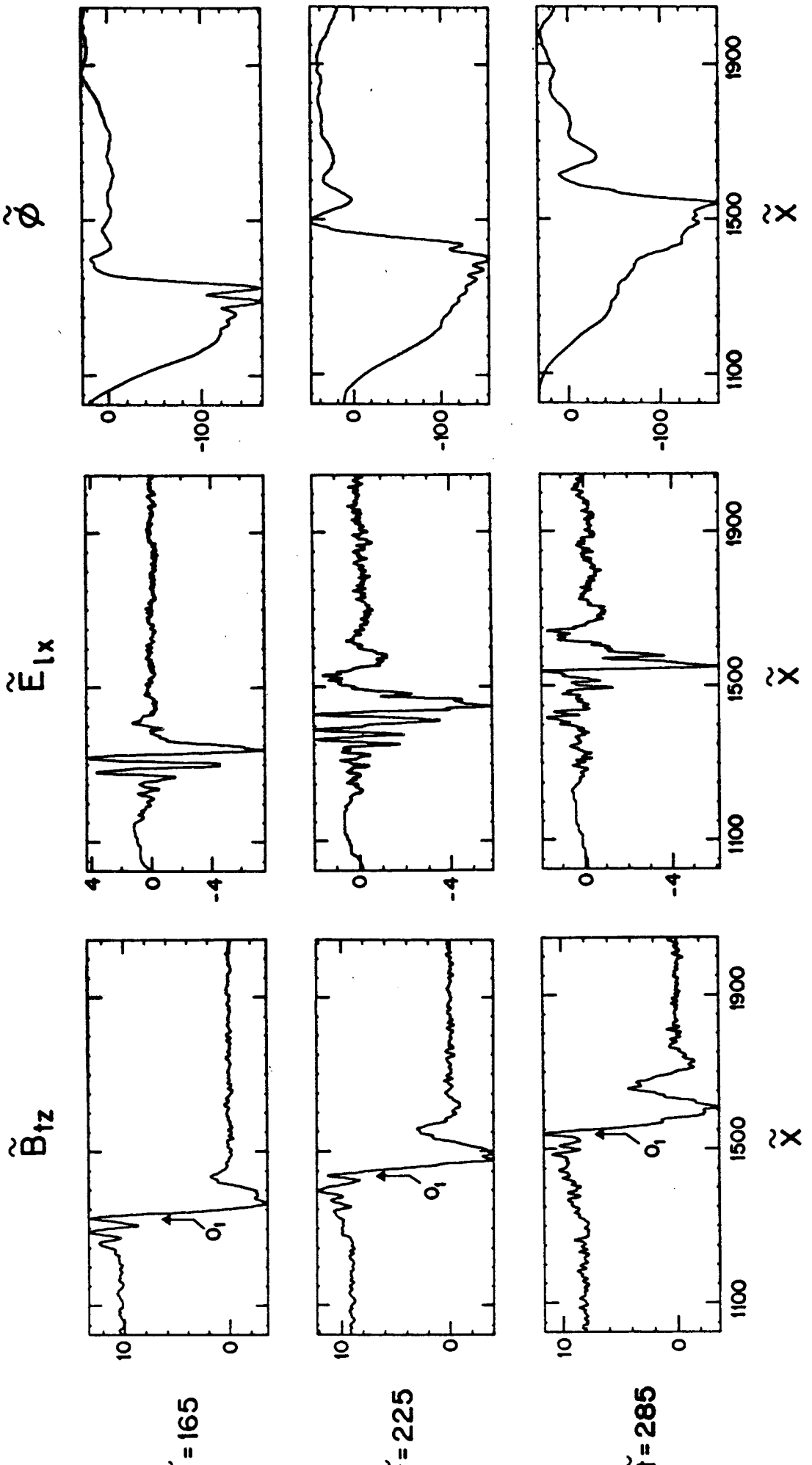
$\tilde{B}_{tz}$
$\tilde{E}_{lx}$
$\tilde{\phi}$
$\tilde{t}$ = 165
$\tilde{t}$ = 225
$\tilde{t}$ = 285
$\tilde{X}$
O_1
10
0
4
-4
-100
1100
1500
1900

Figure 12

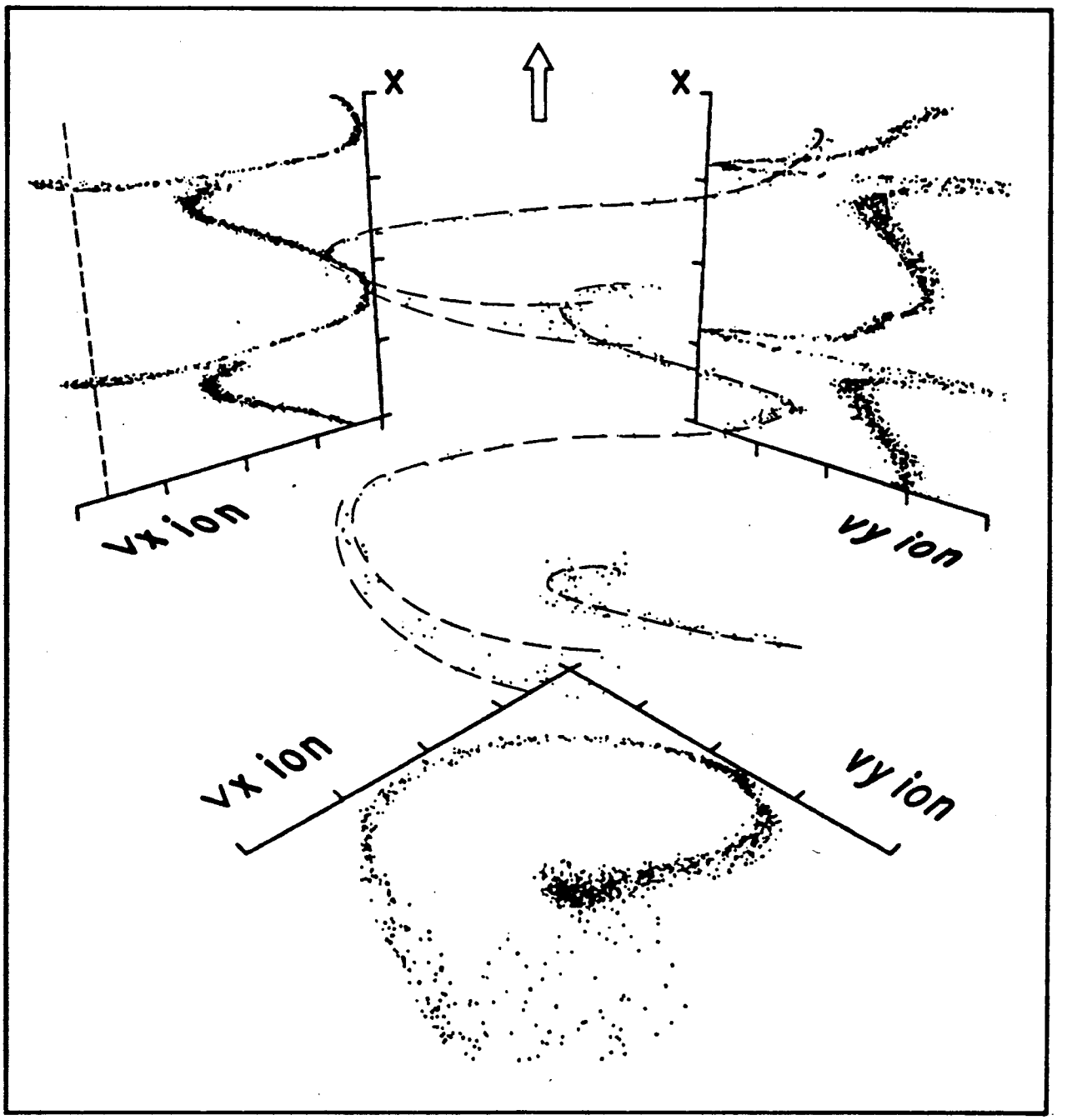

Figure 13

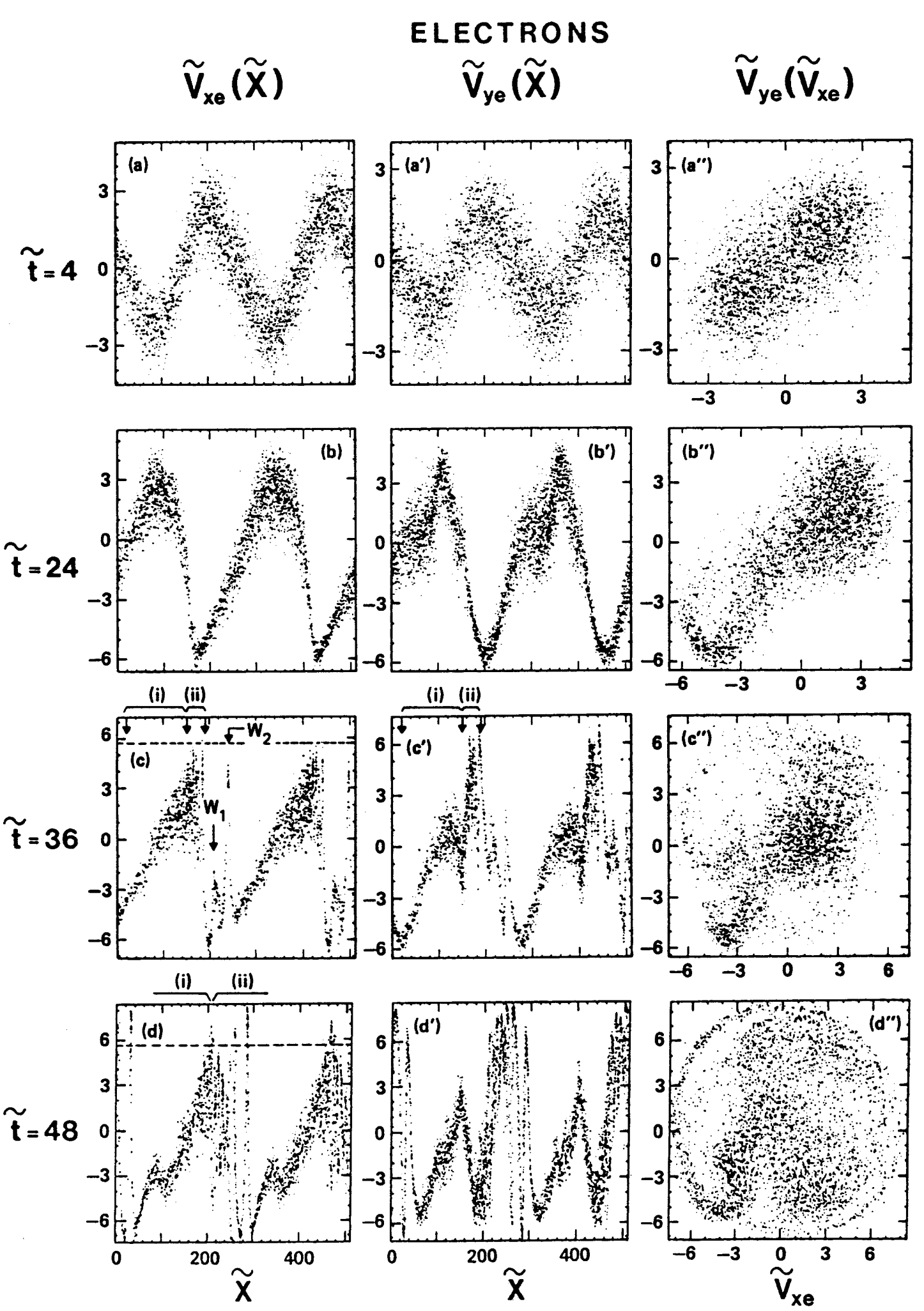
ELECTRONS
$\tilde{V}_{xe}(\tilde{X})$
$\tilde{V}_{ye}(\tilde{X})$
$\tilde{V}_{ye}(\tilde{V}_{xe})$
$\tilde{t}=4$
$\tilde{t}=24$
$\tilde{t}=36$
$\tilde{t}=48$
(a)
(a')
(a'')
(b)
(b')
(b'')
(c)
(c')
(c'')
(d)
(d')
(d'')
(i)
(ii)
W_1
W_2
$\tilde{X}$
$\tilde{V}_{xe}$

Figure 14

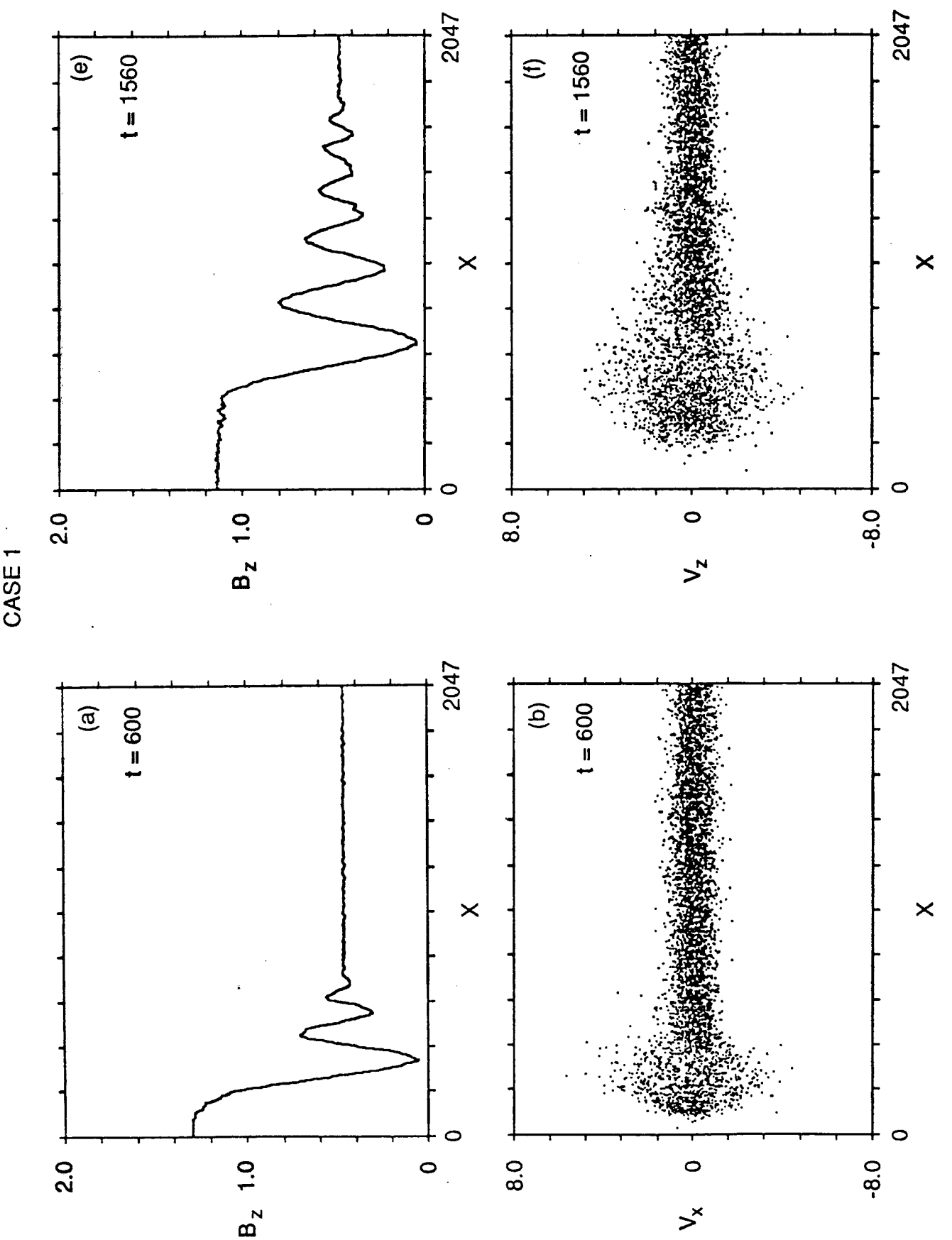

Figure 15 (top)

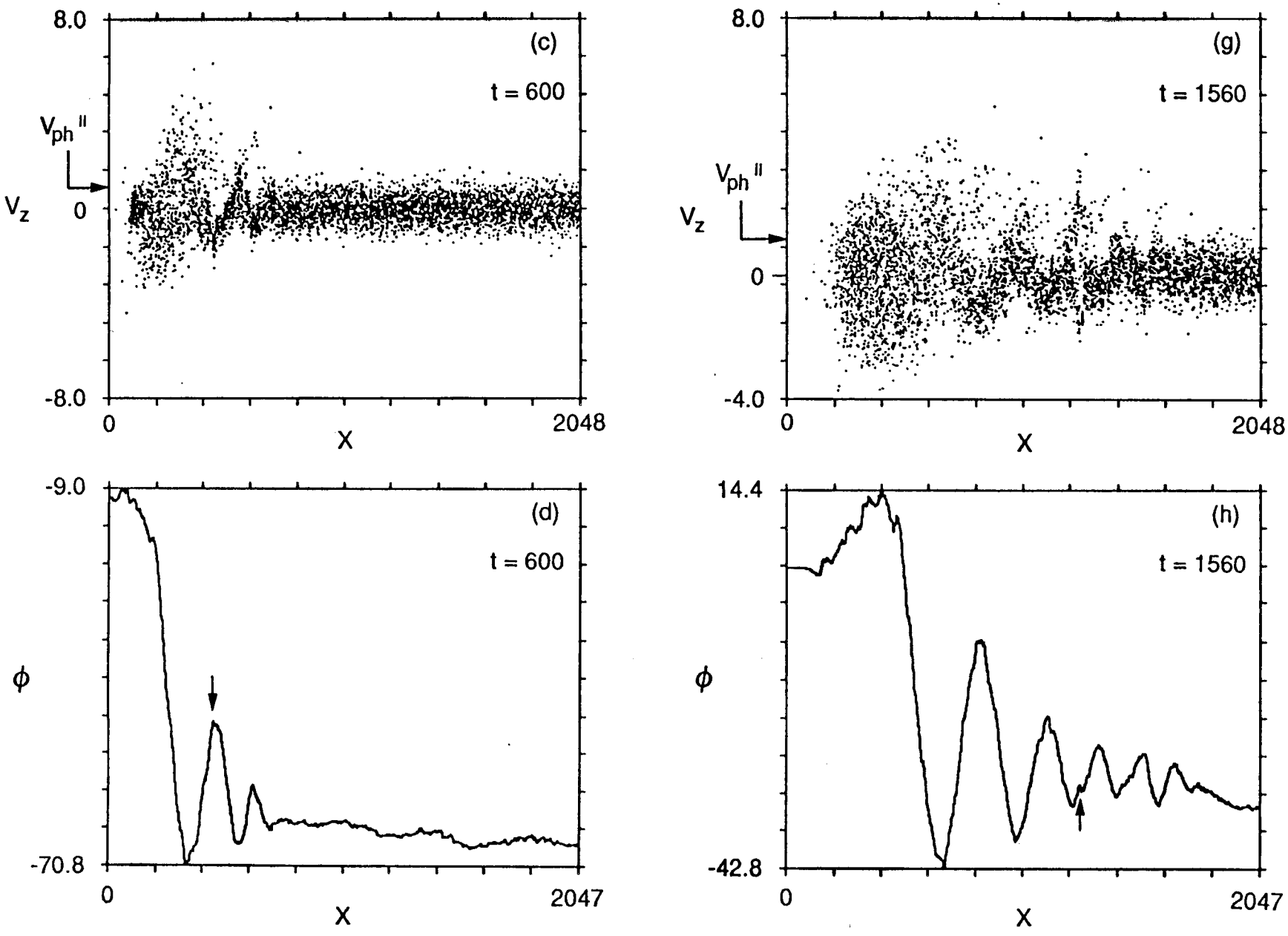

Figure 15(bottom)

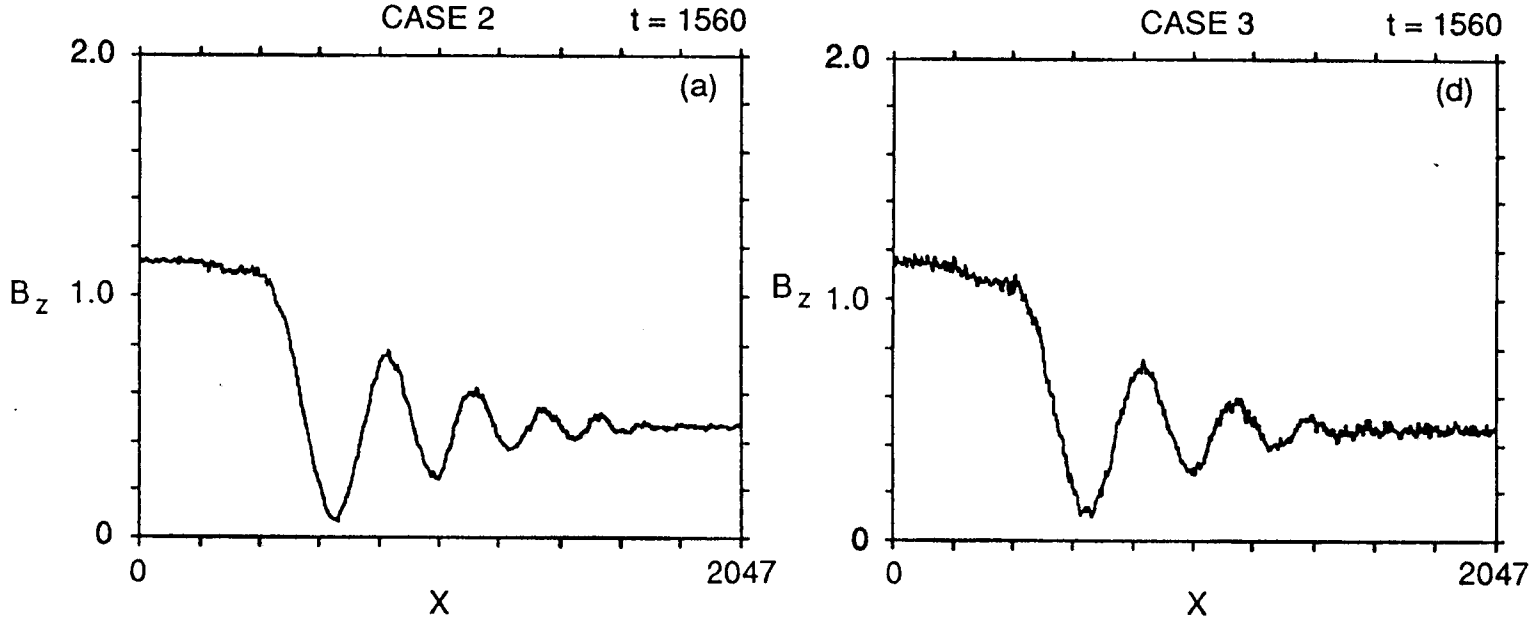

Figure 16